

Chapter 1

Introduction

1.1 Views of the nucleus

In the atom, the nucleus provides the Coulomb field in which negatively charged electrons ($-e$) move independently of each other in single-particle orbitals. The filling of these orbitals explains Mendeleev's periodic table. Thus the valence of the chemical elements as well as the particular stability of the noble gases (He, N, Ar, Kr, Xe and Ra) associated with the closing of shells (Fig. 1.1.1). The dimension of the atom is measured in angstroms ($\text{\AA}=10^{-8}\text{cm}$), and typical energies in eV, the electron mass being $m_e \approx 0.5 \text{ MeV}$ ($\text{MeV}=10^6\text{eV}$).

The atomic nucleus is made out of positively charged protons ($+e$) and of (uncharged) neutrons, nucleons, of mass $\approx 10^3 \text{ MeV}$ ($m_p = 938.3 \text{ MeV}$, $m_n = 939.6 \text{ MeV}$). Nuclear dimensions are of the order of few fermis ($\text{fm}=10^{-13} \text{ cm}$). While the stability of the atom is provided by a source external to the electrons, namely the atomic nucleus, this system is self-bound as a result of the strong interaction of range $a_0 \approx 0.9 \text{ fm}$ and strength $v_0 \approx -100 \text{ MeV}$ acting among nucleons.

1.1.1 The liquid drop and the shell model

While most of the atom is empty space, the density of the atomic nucleus is conspicuous ($\rho = 0.17 \text{ nucleon/fm}^3$). The “closed packed” nature of this system implies a short mean free path as compared to nuclear dimensions. This can be estimated from classical kinetic theory $\lambda \approx (\rho\sigma)^{-1} \approx 1 \text{ fm}$, where $\sigma \approx 2\pi a_0^2$ is the nucleon-nucleon cross section. It seems then natural to liken the atomic nucleus to a liquid drop (Bohr and Kalckar). This picture of the nucleus provided the framework to describe the basic features of the fission process (Meitner and Frisch (1939); Bohr and Wheeler (1939)).

The leptodermic properties of the atomic nucleus are closely connected with the semi-empirical mass formula (Weizsäcker (1935))

$$m(N, Z) = (Nm_n + Zm_p) - \frac{1}{c^2}B(N, Z), \quad (1.1.1)$$

the binding energy being

$$B(N, Z) = \left(b_{vol}A - b_{surf}A^{2/3} - \frac{1}{2}b_{sym}\frac{(N-Z)^2}{A} - \frac{3}{5}\frac{Z^2e^2}{R_c} \right). \quad (1.1.2)$$

The first term is the volume energy representing the binding energy in the limit of large A , $N = Z$ and in the absence of the Coulomb interaction ($b_{vol} \approx 15.6$ MeV). The second term represents the surface energy, where

$$b_{surf} = 4\pi r_0^2 \gamma. \quad (1.1.3)$$

The nuclear radius is written as $R = r_0 A^{1/3}$, with $r_0 = 1.2$ fm, the surface tension energy being $\gamma \approx 0.95$ MeV/fm². The third term in (1.1.2) is the symmetry term which reflects the tendency towards stability for $N = Z$, with $b_{sym} = 50$ MeV. The symmetry energy can be divided into a kinetic and a potential energy part. A simple estimate of the kinetic energy part can be obtained by making use of the Fermi gas model which gives $(b_{sym})_{kin} \approx (2/3)\epsilon_F \approx 25$ MeV ($\epsilon_F \approx 36$ MeV). Consequently,

$$V_1 = (b_{sym})_{pot} = b_{sym} - (b_{sym})_{kin} \approx 25 \text{ MeV}. \quad (1.1.4)$$

The last term of (1.1.2) is the Coulomb energy corresponding to a uniformly charged sphere of radius $R_c = 1.24A^{1/3}$ fm.

When, in a heavy-ion reaction, two nuclei come within the range of the nuclear forces, the trajectory of relative motion will be changed by the attraction which will act between the nuclear surfaces. This surface interaction is a fundamental quantity in all heavy ion reactions. Assuming two spherical nuclei at a relative distance $r_{AA} = R_a + R_A$, where R_a and R_A are the corresponding half-density radii, the force acting between the two surfaces is

$$\left(\frac{\partial U_{AA}^N}{\partial r} \right)_{r_{AA}} = 4\pi\gamma \frac{R_a R_A}{R_a + R_A} \quad (1.1.5)$$

This result allows for the calculation of the ion-ion (proximity) potential which, supplemented with a position dependent absorption, can be used to accurately describe heavy ion reactions¹.

In such reactions, not only elastic processes are observed, but also anelastic processes in which one, or both surfaces of the interacting nuclei are set into vibration (Fig. 1.1.2). The restoring force parameter associated with oscillations of multipolarity λ is

$$C_\lambda = (\lambda - 1)(\lambda + 2)R_0^2\gamma - \frac{3}{2\pi} \frac{\lambda - 1}{2\lambda + 1} \frac{Z^2e^2}{R_c}, \quad (1.1.6)$$

where the second term corresponds to the contribution of the Coulomb energy to C_λ . Assuming the flow associated with surface vibration to be irrotational, the

¹Broglia and Winther (2004) and refs. therein.

associated inertia for small amplitude oscillations is,

$$D_\lambda = \frac{3}{4\pi} \frac{1}{\lambda} AMR^2, \quad (1.1.7)$$

the energy of the corresponding mode being

$$\hbar\omega_\lambda = \hbar \sqrt{\frac{C_\lambda}{D_\lambda}}. \quad (1.1.8)$$

The label λ stands for the angular momentum of the vibrational mode, μ being its third component (see Eq. (1.2.1)). Aside from λ, μ , surface vibrations can also be characterized by an integer $n (= 1, 2, \dots)$, an ordering number indicating increasing energy. For simplicity, a single common label α will also be used.

Experimental information associated with low-energy quadrupole vibrations, namely $\hbar\omega_2$ and the electromagnetic transition probabilities $B(E2)$, allow to determine C_2 and D_2 . The resulting C_2 values exhibit variations by more than a factor of 10 both above and below the liquid-drop estimate. The observed values of D_2 are large as compared with the mass parameter for irrotational flow.

A picture apparently antithetic to that of the liquid drop, the shell model, emerged from the study of experimental data, plotting them against either the number of protons (atomic number), or the number of neutrons in the nuclei, rather than against the mass number. One of the main nuclear features which led to the development of the shell model was the study of the stability and abundance of nuclear species and the discovery of what are usually called magic numbers (Elsasser (1933); Mayer (1948); Haxel et al. (1949)). What makes a number magic is that a configuration of a magic number of neutrons, or of protons, is unusually stable whatever the associated number of other nucleons is (Mayer (1949); Mayer and Teller (1949)).

The strong binding of a magic number of nucleons and weak binding for one more reminds, only relatively weaker, the results displayed in Fig. 1.1.1 concerning the atomic stability of rare gases. In the nuclear case, at variance with the atomic case, the spin-orbit coupling play an important role, as can be seen from the level scheme shown in Fig. 1.1.3, obtained by assuming that nucleons move independently of each other in an average potential of spherical symmetry.

A closed shell, or a filled level, has angular momentum zero. Thus, nuclei with one nucleon outside (missing from) closed shell, should have the spin and parity of the orbital associated with the odd nucleon (-hole), a prediction confirmed by the data (available at that time) throughout the mass table. Such a picture implies that the nucleon mean free path is large compared to nuclear dimensions.

The systematic studies of the binding energies leading to the shell model found also that the relation (1.1.2), has to be supplemented to take into account the fact that nuclei with both odd number of protons and of neutrons are energetically unfavored compared with even-even ones (inset Fig. 1.1.1) by a quantity of the order of $\delta \approx 33 MeV/A^{3/4}$ called the pairing energy².

²Connecting with further developments associated with the BCS theory of superconductivity

The low-lying excited state of closed shell nuclei can be interpreted as a rule, as harmonic quadrupole or octupole collective vibrations (Fig. 1.1.4) described by the Hamiltonian³

$$H_{coll} = \sum_{\lambda\mu} \left(\frac{1}{2D_\lambda} |\Pi_{\lambda\mu}|^2 + \frac{C_\lambda}{2} |\alpha_{\lambda\mu}|^2 \right) \quad (1.1.9)$$

Following Dirac (1930) one can describe the oscillatory motion introducing boson creation (annihilation) operator $\Gamma_{\lambda\mu}^\dagger$ ($\Gamma_{\lambda\mu}$) obeying

$$[\Gamma_\alpha, \Gamma_{\alpha'}^\dagger] = \delta(\alpha, \alpha'), \quad (1.1.10)$$

leading to

$$\hat{\alpha}_{\lambda\mu} = \sqrt{\frac{\hbar\omega_\lambda}{2C_\lambda}} (\Gamma_{\lambda\mu}^\dagger + (-1)^\mu \Gamma_{\lambda-\mu}), \quad (1.1.11)$$

and a similar expression for the conjugate momentum variable $\hat{\Pi}_{\lambda\mu}$, resulting in

$$\hat{H}_{coll} = \sum \hbar\omega_\lambda ((-1)^\mu \Gamma_{\lambda\mu}^\dagger \Gamma_{\lambda-\mu} + 1/2). \quad (1.1.12)$$

The frequency is $\omega_\lambda = (C_\lambda/D_\lambda)^{1/2}$, while $(\hbar\omega_\lambda/2C_\lambda)^{1/2}$ is the amplitude of the zero-point fluctuation of the vacuum state $|0\rangle_B, |n_{\lambda\mu} = 1\rangle = \Gamma_{\lambda\mu}^\dagger |0\rangle_B$ being the one-phonon state. To simplify the notation, in many cases one writes $|n_\alpha = 1\rangle$.

The ground and low-lying states of nuclei with one nucleon outside closed shell can be described by the Hamiltonian

$$H_{sp} = \sum_\nu \epsilon_\nu a_\nu^\dagger a_\nu, \quad (1.1.13)$$

where $a_\nu^\dagger (a_\nu)$ is the single-particle creation (annihilation) operator,

$$|\nu\rangle = a_\nu^\dagger |0\rangle_F, \quad (1.1.14)$$

being the single-particle state of quantum numbers $\nu (\equiv nljm)$ and energy ϵ_ν , while $|0\rangle_F$ is the Fermion vacuum. It is of notice that

$$[H_{coll}, \Gamma_{\lambda'\mu'}^\dagger] = \hbar\omega_{\lambda'} \Gamma_{\lambda'\mu'}^\dagger \quad (1.1.15)$$

and

$$[H_{sp}, a_{\nu'}^\dagger] = \epsilon_{\nu'} a_{\nu'}^\dagger. \quad (1.1.16)$$

(Bardeen et al. (1957a,b)) and its extension to the atomic nucleus (Bohr et al. (1958)), the quantity δ is identified with the pairing gap Δ parametrized according to $\Delta = 12 \text{MeV}/\sqrt{A}$ (Bohr and Mottelson (1969)). It is of notice that for typical superfluid nuclei like ^{120}Sn , the expression of δ leads to a numerical value which can be parametrized as $\delta \approx 10 \text{ MeV}/\sqrt{A}$.

³Classically $\Pi_{\lambda\mu} = D_\lambda \dot{\alpha}_{\lambda\mu}$.

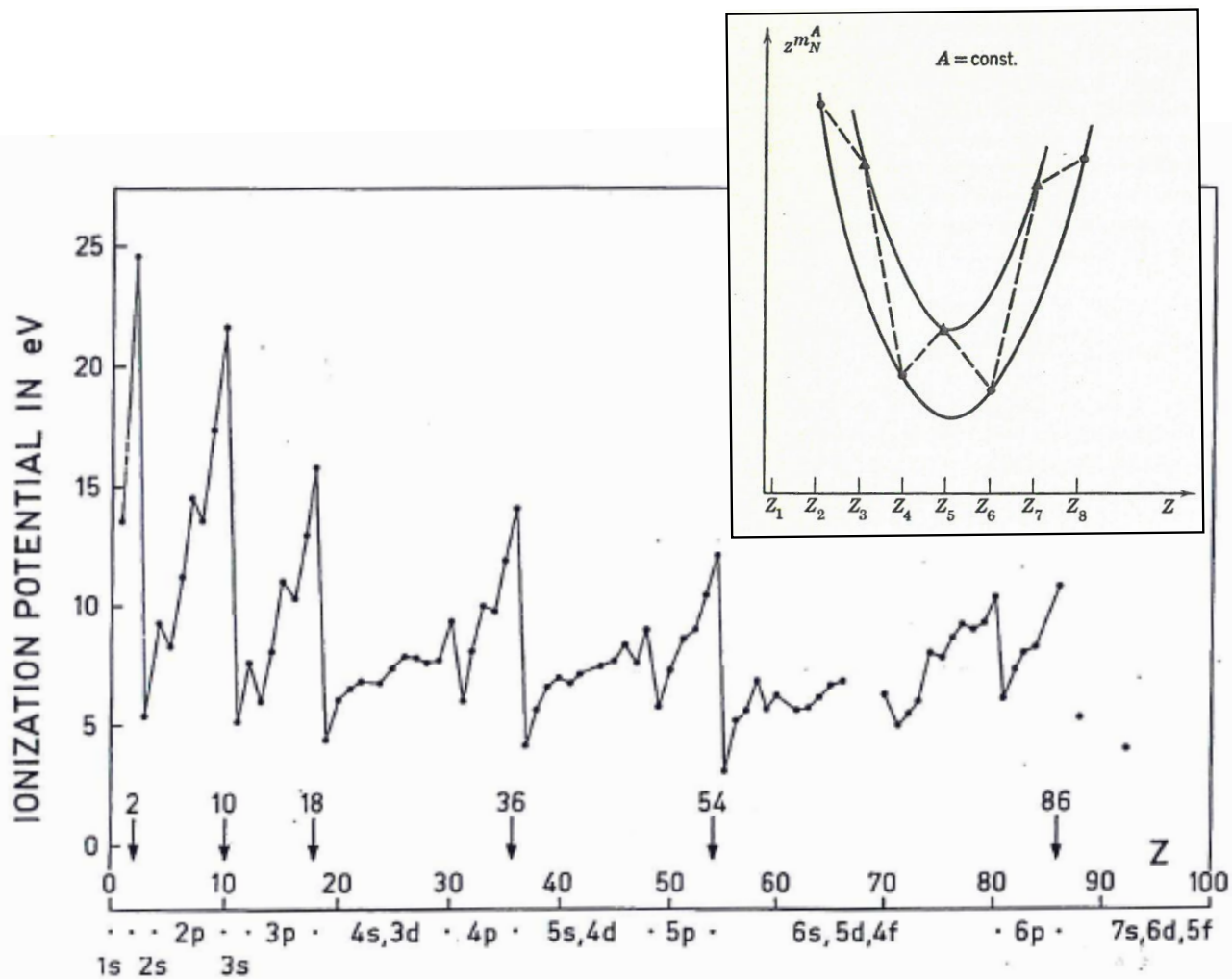


Figure 1.1.1: The values of the atomic ionization potentials. The closed shells, corresponding to electron number 2(He), 10(Ne), 18(Ar), 36(Kr), 54(Xe), and 86(Ra), are indicated. After Bohr and Mottelson (1969). In the inset, masses of nuclei with even A are shown (after Mayer and Jensen (1955)).

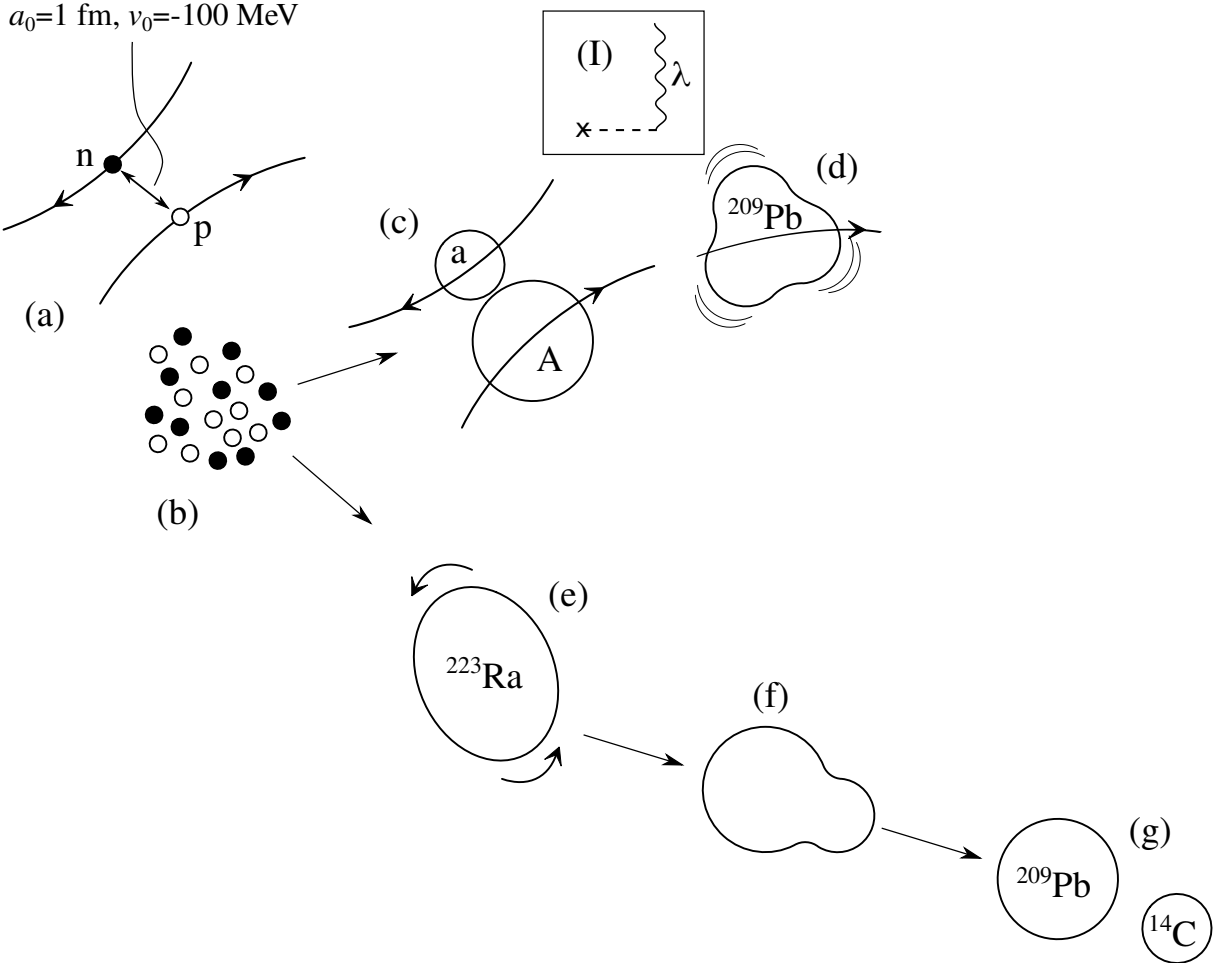


Figure 1.1.2: Emergent properties (collective nuclear models) (a) Nucleon-Nucleon (NN) interaction in a scattering experiment; (b) assembly of a swarm of nucleons condensing into drops of nuclear matter, examples shown in (c) and (e); (c) anelastic heavy ion reaction $a + A \rightarrow a + A^*$ setting the nucleus A into an octupole surface oscillations (d); in inset (I) the time-dependent nuclear plus Coulomb fields associated with the reaction (c) is represented by a cross followed by a dashed line, while the wavy line labeled λ describes the propagation of the surface vibration shown in (d), time running upwards; (e) another possible outcome of nucleon condensation: the (weakly) quadrupole deformed nucleus ^{223}Ra which can rotate as a whole with moment of inertia smaller than the rigid moment of inertia, but much larger than the irrotational one; (f) the zero point fluctuations (quadrupole ($\lambda = 2$), octupole ($\lambda = 3$), etc.) can get with a small but finite probability ($P \approx 10^{-10}$) spontaneously in phase and produce a neck-in (saddle conformation) leading eventually to the (exotic) decay mode $^{223}\text{Ra} \rightarrow ^{209}\text{Pb} + ^{14}\text{C}$, as experimentally observed (g).

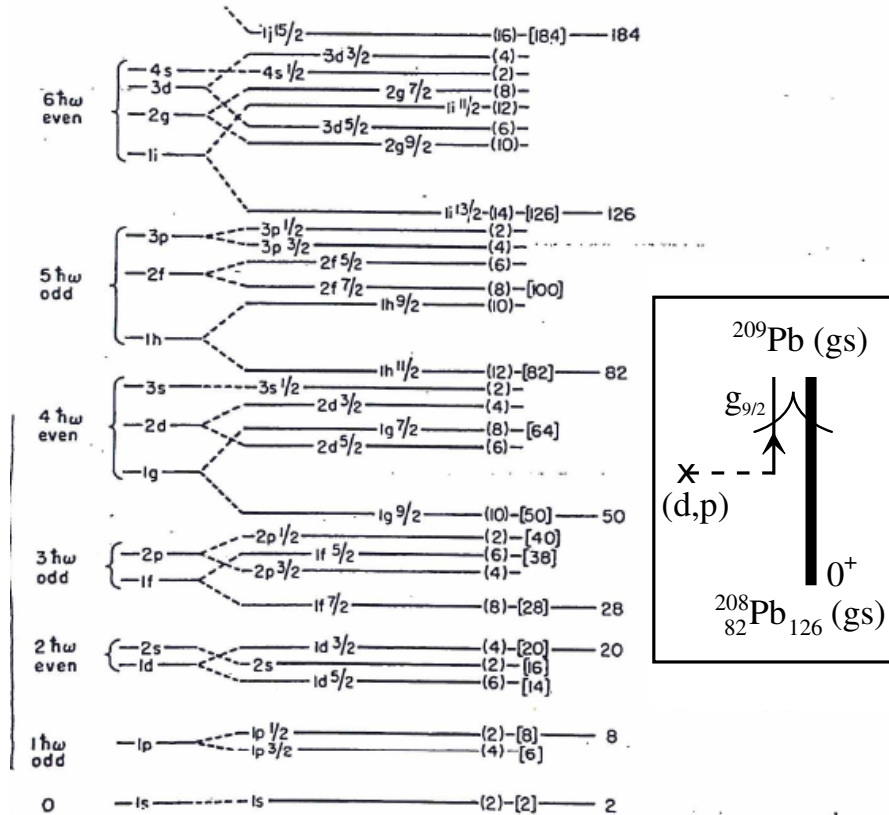


Figure 1.1.3: To the left (first column), the sequence of levels of the harmonic oscillator potential labeled with the total oscillator quantum number and parity $\pi = (-1)^N$. The next column shows the splitting of major shell degeneracies obtained using a more realistic potential (Woods-Saxon), the quantum number being the number of radial nodes of the associated single-particle s, p, d , etc., states. The levels shown at the center result when a spin-orbit term is also considered, the quantum numbers nlj characterizing the states of degeneracy $(2j+1)$ ($j = l \pm 1/2$) (After Mayer (1963)). In the inset, a schematic graphical representation of the reaction $^{208}_{82}\text{Pb}_{126}(d, p)^{209}\text{Pb}(\text{gs})$ is shown. A cross followed by a horizontal dashed line represents the (d, p) field, while a single arrowed line describes the odd nucleon moving in the $g_{9/2}$ orbital above the $N = 126$ shell closure (and belonging to the $N = 6$ major shell) drawn as a bold line labeled 0^+ (after Bohr and Mottelson (1969)).

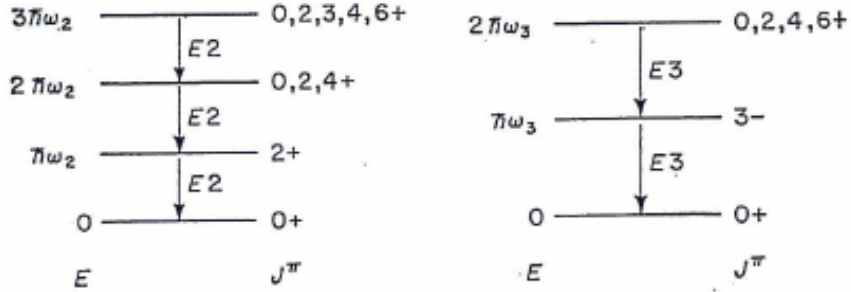


Figure 1.1.4: Schematic representation of harmonic quadrupole and octupole liquid drop collective surface vibrational modes (after Rowe (1970)).

This is an obvious outcome resulting from the bosonic

$$[\Gamma_\alpha, \Gamma_{\alpha'}^\dagger] = \delta(\alpha, \alpha') \quad (1.1.17)$$

and fermionic

$$\{a_\nu, a_{\nu'}^\dagger\} = \delta(\nu, \nu') \quad (1.1.18)$$

commutation (anti-commutation) relations.

Both the existence of drops of nuclear matter displaying collective surface vibrations, and of independent-particle motion in a self-confining mean field are emergent properties not contained in the particles forming the system, neither in the NN -force, but on the fact that these particles behave according to the rules of quantum mechanics, move in a confined volume and that there are many of them.

Generalized rigidity as measured by the inertia parameter D_λ , as well as surface tension closely connected to the restoring force C_λ , implies that acting on the system with an external time-dependent (nuclear and/or Coulomb) field, the system reacts as a whole. This behavior is to be found nowhere in the properties of the nucleons, nor in the nucleon-nucleon scattering phase shifts consistent with Yukawa's predictions of the existence of a π -meson as the carrier of the strong force acting among nucleons.

Similarly, the fact that nuclei probed through fields which change in one unit particle number (e.g. (d, p) and (p, d) reactions) react in term of independent particle motion, feeling the pushings and pullings of the other nucleons only when trying to leave the nucleus, is not apparent in the detailed properties of the NN -forces, not even in those carrying the quark-gluon input. Within this context, independent particle motion can be considered a *bona fide* emergent property.

Collective surface vibrations and independent particle motion are examples of what are called elementary modes of excitation in many-body physics, and collective variables in soft-matter physics.

1.2 The particle-vibration coupling

The oscillation of the nucleus under the influence of surface tension implies that the potential $U(R, r)$ in which nucleons move independently of each other change with time. For low-energy collective vibrations this change is slow as compared with single-particle motion. Within this scenario the nuclear radius can be written as

$$R = R_0 \left(1 + \sum_{LM} \alpha_{LM} Y_{LM}^*(\hat{r}) \right) \quad (1.2.1)$$

Assuming small amplitude motion,

$$U(r, R) = U(r, R_0) + \delta U(r), \quad (1.2.2)$$

where

$$\delta U = -\kappa \hat{a} \hat{F}, \quad (1.2.3)$$

and

$$\hat{F} = \sum_{\nu_1 \nu_2} \langle \nu_1 | F | \nu_2 \rangle a_{\nu_1}^\dagger a_{\nu_2}, \quad (1.2.4)$$

while

$$F = \frac{R_0}{\kappa} \frac{\partial U}{\partial r} Y_{LM}^*(\hat{r}). \quad (1.2.5)$$

The coupling between surface oscillation and single-particle motion, namely the particle vibration coupling (PVC) Hamiltonian δU (Fig. 1.2.1) is a consequence of the overcompleteness of the basis. Diagonalizing δU making use of the graphical (Feynman) rules of nuclear field theory (NFT) to be discussed in following Chapter, one obtains structure results which can be used in the calculation of transition probabilities and reaction cross sections, quantities which can be compared with experimental findings.

In fact, within the framework of NFT, single-particles are to be calculated as the Hartree–Fock solution of the NN -interaction $v(|\mathbf{r} - \mathbf{r}'|)$ (Fig. 1.2.2), in particular

$$U(r) = \int d\mathbf{r}' \rho(r') v(|\mathbf{r} - \mathbf{r}'|) \quad (1.2.6)$$

being the Hartree field⁴ expressing the selfconsistency between density ρ and potential U (Fig. 1.2.2 (b) (1) and (3)), while vibrations are to be calculated in the

⁴To this potential one has to add the Fock potential resulting from the fact that nucleons are fermions. This exchange potential (Fig. 1.2.2 (b) (2 and 4)) is essential in the determination of single-particle energies and wavefunctions. Among other things, it takes care of eliminating the nucleon self interaction from the Hartree field.

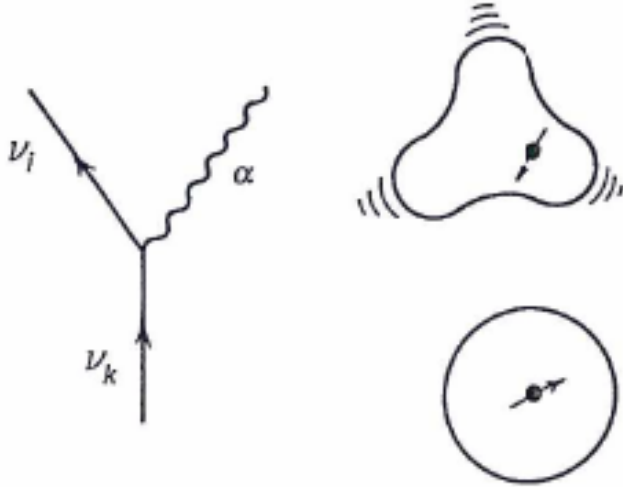


Figure 1.2.1: Graphical representation of process by which a fermion, bouncing inelastically off the surface, sets it into vibration. Particles are represented by an arrowed line pointing upwards which is also the direction of time, while the vibration is represented by a wavy line. In the cartoon to the right, the black dot represents a nucleon moving in a spherical mean field of which it excites an octupole vibration after bouncing off the surface.

Random Phase Approximation (RPA) making use of the same interaction⁵ (Fig. 1.2.3), extending the selfconsistency to fluctuations $\delta\rho$ of the density and δU of the mean field, that is,

$$\delta U(r) = \int d\mathbf{r}' \delta\rho(r') v(|\mathbf{r} - \mathbf{r}'|). \quad (1.2.7)$$

Making use of the solution to this relation one obtains the transition density $\delta\rho$. The matrix elements $\langle n_\lambda = 1, \nu_i | \delta\rho | \nu_k \rangle$ provide the particle-vibration coupling strength to work out the variety of coupling processes between single-particle and collective motion (Fig. 1.2.1). That is, the matrix element of the PVC Hamiltonian H_c . Diagonalizing

$$H = H_{HF} + H_{RPA} + H_c + v, \quad (1.2.8)$$

applying in the basis of single-particle and collective modes, that is solutions of H_{HF} and of H_{RPA} respectively, the NFT rules (see next chapter) one obtains a solution of the total Hamiltonian. Concerning the rules of NFT, they codify the way in which H_c (three-point vertices) and v (four-point vertices) are to be treated to all

⁵The sum of the so called ladder diagrams (see Fig. 1.2.3) are taken into account to infinite order in RPA. This is the reason why bubble contributions in the diagonalization of Eq. (1.2.8) are not allowed in NFT, being already contained in the basis states (see next chapter, Sect. 2.7 ??).

orders of perturbation theory. Also which processes (diagrams) are not allowed because they will imply overcounting of correlations already included in the basis states⁶.

Because of quantal zero point fluctuations, a nucleon propagating in the nuclear medium moves through a cloud of bosonic virtual excitations to which it couples becoming dressed and acquiring effective mass, charge, etc. (Fig. 1.2.4). Vice versa, vibrational modes can become renormalized through the coupling to dressed nucleons which, in intermediate virtual states, can exchange the vibrations which produce their clothing, with the second fermion (hole state). Such a process leads to a renormalization of the PVC vertex⁷ (Fig. 1.2.5), as well as of the bare NN -interaction, in particular 1S_0 component (bare pairing interaction)⁸.

The analytic procedures equivalent to the diagrammatic ones to obtain the HF (Fig. 1.2.2) and RPA (Fig. 1.2.3) solutions associated with the bare NN -interaction v is provided by the relations (1.1.16) and (1.1.15) respectively, replacing the corresponding Hamiltonians by $(T + v)$, where T is the kinetic energy operator. The phonon operator associated with surface vibrations is defined as,

$$\Gamma_\alpha^\dagger = \sum_{ki} X_{ki}^\alpha \Gamma_{ki}^\dagger + Y_{ki}^\alpha \Gamma_{ki}, \quad (1.2.9)$$

the normalization condition being,

$$[\Gamma_\alpha, \Gamma_\alpha^\dagger] = \sum_{ki} (X_{ki}^{\alpha 2} - Y_{ki}^{\alpha 2}) = 1. \quad (1.2.10)$$

The operator $\Gamma_{ki}^\dagger = a_k^\dagger a_i (\epsilon_k > \epsilon_F, \epsilon_i \leq \epsilon_F)$ creates a particle-hole excitation acting on the HF vacuum state $|0\rangle_F$. It is assumed that

$$[\Gamma_{ki}, \Gamma_{k'i'}^\dagger] = \delta(k, k')\delta(i, i'). \quad (1.2.11)$$

Within this context, RPA is a harmonic, quasi-boson approximation.

From being antithetic views of the nuclear structure, a proper analysis of the experimental data testifies to the fact that the collective and the independent particle pictures of the nuclear structure require and support each other (Bohr, A. and Mottelson (1975)). To obtain a quantitative description of nucleon motion and nuclear phonons (vibrations), one needs a proper description of the k - and ω -dependent “dielectric” function of the nuclear medium, in a similar way in which a proper

⁶A simple, although not directly related but only in a general way, example is provided by Eq. (2A-31) of Bohr and Mottelson (1969) i.e. $G = \frac{1}{4} \sum_{\nu_1 \nu_2 \nu_3 \nu_4} \langle \nu_3 \nu_4 | G | \nu_1 \nu_2 \rangle_a a^\dagger(\nu_4) a^\dagger(\nu_3) a(\nu_1) a(\nu_2) = \frac{1}{2} \sum_{\nu_1 \nu_2 \nu_3 \nu_4} \langle \nu_3 \nu_4 | G | \nu_1 \nu_2 \rangle_a a^\dagger(\nu_4) a^\dagger(\nu_3) a(\nu_1) a(\nu_2)$ where $\langle \cdot \rangle_a$ is the antisymmetric matrix element.

⁷Bertsch et al. (1983); Barranco et al. (2004) and refs. therein. It is to be noted that in the case in which the renormalized vibrational modes, i.e. the initial and final wavy lines in Fig. 1.2.5 have angular momentum and parity $\lambda^\pi = 0^+$, and one uses a model in which there is symmetry between the particle and the hole subspaces, the four diagrams sum to zero, because of particle (gauge) conservation.

⁸See e.g. Brink, D. and Broglia (2005) Ch. 10 and references therein.

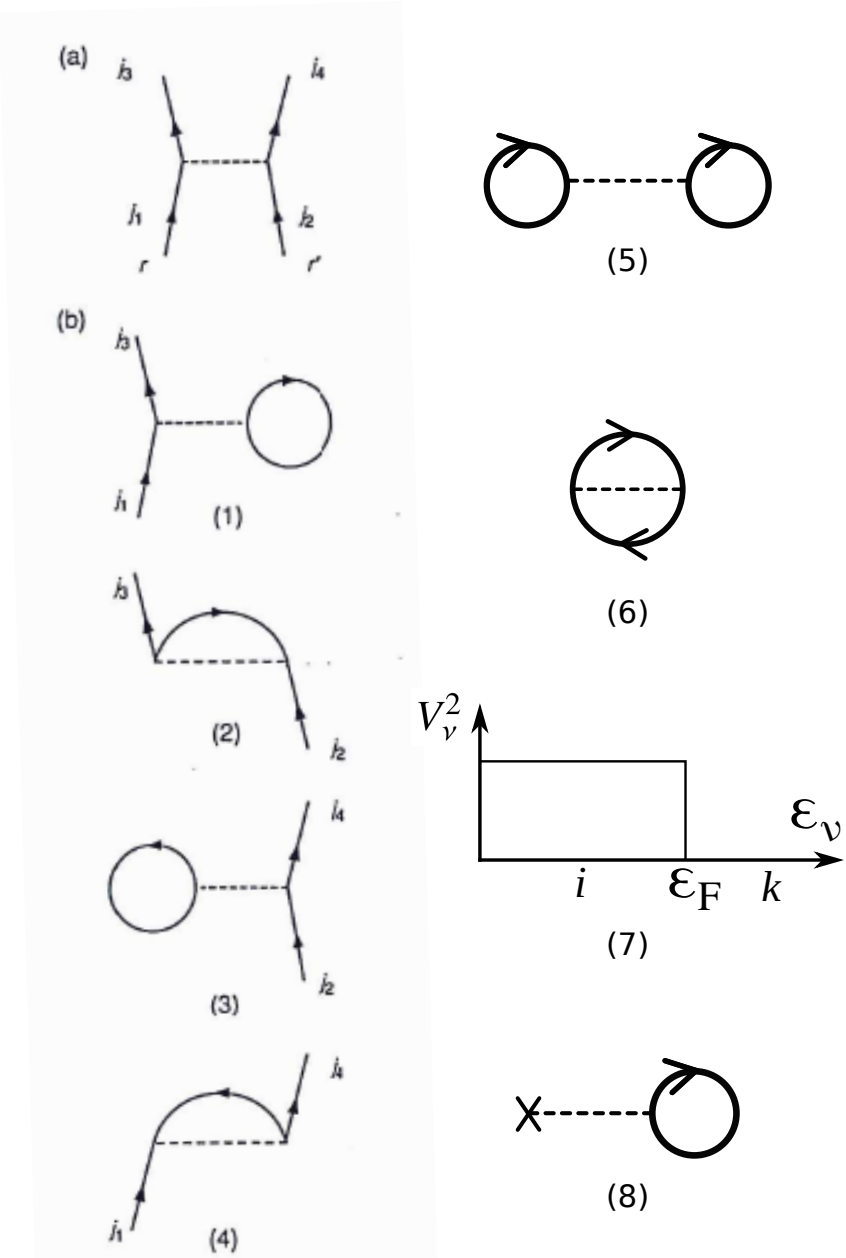


Figure 1.2.2: **(a)** Scattering of two nucleons through the bare NN -interaction; **(b)** (1) and (3): Contributions to the (direct) Hartree potential; (2) and (4): contributions to the (exchange) Fock potential. In (5) and (6) the ground state correlations associated with the Hartree- and the Fock-terms are displayed. (7) States $|i\rangle$ ($\epsilon_i \leq \epsilon_F$) are occupied with probability $V_i^2 = 1$. States $|k\rangle$ ($\epsilon_k > \epsilon_F$) are empty $V_k^2 = 1 - U_k^2$. (8) Nuclear density, the density operator being represented by a cross followed by a dashed horizontal line. (After Brink, D. and Broglia (2005)).

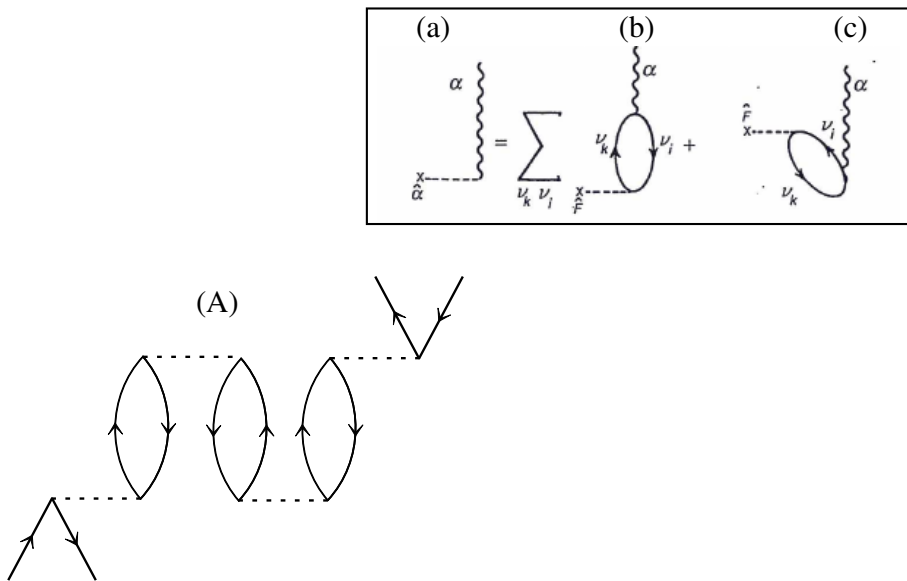


Figure 1.2.3: (A) typical Feynman diagram diagonalizing the NN -interaction $v(|\mathbf{r} - \mathbf{r}'|)$ (horizontal dashed line) in a particle-hole basis provided by the Hartree-Fock solution of v , in the harmonic approximation (RPA). Bubbles going forward in time (inset (b); leading to the amplitudes $X_{ki}^\alpha = \frac{\Lambda_\alpha \langle \tilde{i}|F|k\rangle}{(\epsilon_k - \epsilon_i) - \hbar\omega_\alpha}$) are associated with configuration mixing of particle-hole states. Bubbles going backwards in time (inset (c); leading to the amplitudes $Y_{ki}^\alpha = -\frac{\Lambda_\alpha \langle \tilde{i}|F|k\rangle}{(\epsilon_k - \epsilon_i) + \hbar\omega_\alpha}$) are associated with zero point motion (fluctuations ZPF) of the ground state (term $(1/2)\hbar\omega$ for each degree of freedom in Eq. 1.1.12). The self consistent solutions of A , eigenstates of the dispersion relation $\sum_{ki} \frac{2(\epsilon_k - \epsilon_i) \langle \tilde{i}|F|k\rangle^2}{(\epsilon_k - \epsilon_i)^2 - (\hbar\omega_\alpha)^2} = 1/\kappa$ are represented by a wavy line (inset (a)), that is a collective mode which can be viewed as a correlated particle (arrowed line going upward)- hole (arrowed line going downward) excitation.

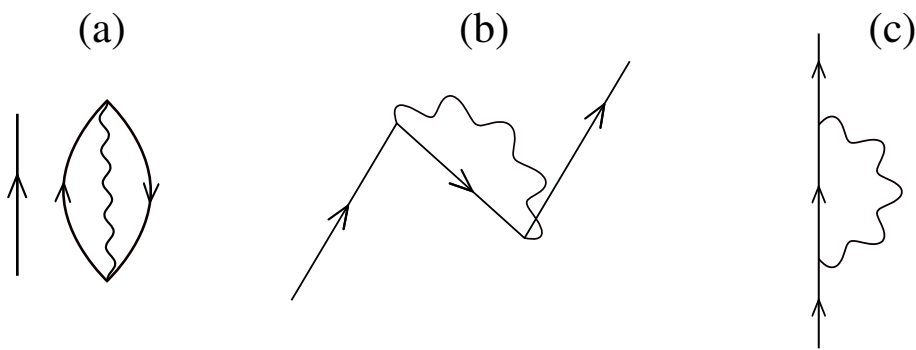


Figure 1.2.4: **(a)** a nucleon (single arrowed line pointing upward) moving in presence of the zero point fluctuation of the nuclear ground state associated with a collective surface vibration; **(b)** Pauli principle leads to a dressing process of the nucleon; **(c)** time ordering gives rise to the second possible lowest order clothing process (time assumed to run upwards).

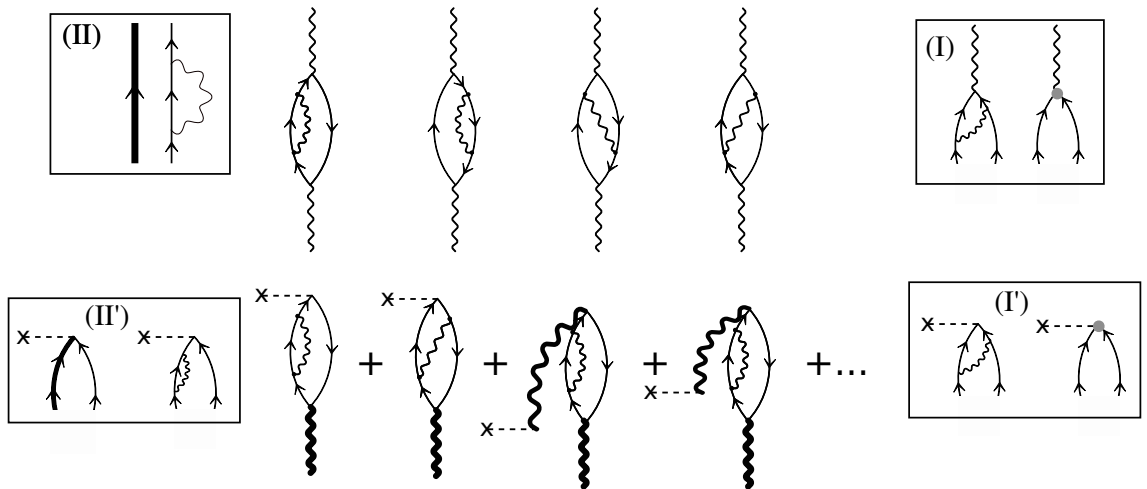


Figure 1.2.5: (Upper part) Examples of renormalization processes dressing a surface collective vibrational state. (Lower part) Intervening with an external electromagnetic field ($E\lambda$: cross followed by dashed horizontal line; bold wavy lines, renormalized vibration of multipolarity λ) the $B(E\lambda)$ transition strength can be measured. In insets (I) and (I'), the hatched circle in the diagram to the right stands for the renormalized PVC strength resulting from the processes described by the diagrams to the left (vertex corrections). In (II) and (II') the bold face arrowed curve represent (left diagram) the motion of a nucleon of effective mass m^* in a potential $(m/m^*)U(r)$, generated by the self-energy process shown to the right, $U(r)$ being the potential describing the motion of nucleons (drawn as a thin arrowed line) of bare mass m (see e.g. Brink, D. and Broglia (2005) App. B).

description of the reaction processes used as probes of the nuclear structure requires the use of the optical potential (continuum “dielectric” function). The NFT solution of (1.2.8) provides all the elements to calculate the structure properties of nuclei, and also the optical potential needed to describe nucleon-nucleus as well as the nucleus-nucleus scattering and reaction processes. It furthermore shows that both single-particle and vibrational elementary modes of excitation emerge from the same properties of the NN -interaction, the main task being that of relating these modes with the observables. Namely with the absolute differential cross sections, in keeping with the central role played by the quantal many-body renormalization processes and associated emergent properties. Renormalization which acts on par on the radial dependence of the wavefunctions (formfactors) and on the single-particle content of the orbitals involved in the reaction process under discussion. In other words, structure ad reactions are to be treated on equal footing⁹.

The development of experimental techniques and associated hardware has allowed for the identification of a rich variety of elementary modes of excitation aside from collective surface vibrations and of independent particle motion: quadrupole and octupole rotational bands, giant resonance of varied multipolarity and isospin, as well as pairing vibrations and rotation, together with giant pairing vibrations of transfer quantum number $\beta \pm 2$. Modes which can be specifically excited in inelastic and Coulomb excitation processes, and one- and two-particle transfer reactions.

1.3 Pairing vibrations

Let us introduce this new type of elementary mode of excitation by making a parallel with quadrupole surface vibrations within the framework of RPA, namely

$$[(H_{sp} + H_i), \Gamma_{k'i'}^\dagger] = \hbar\omega_\alpha \Gamma_{k'i'}^\dagger, \quad (1.3.1)$$

where for simplicity we use, instead of v , a quadrupole-quadrupole separable interaction ($i = QQ$) defined as

$$H_{QQ} = -\kappa Q^\dagger Q \quad (1.3.2)$$

with

$$Q^\dagger = \sum_{ki} \langle k | r^2 Y_{2\mu} | i \rangle a_k^\dagger a_i, \quad (1.3.3)$$

while H_{sp} and Γ_α^\dagger are defined in (1.1.13) and (1.2.9) supplemented by (1.2.10).

In connection with the pairing energy mentioned in relation with the inset to Fig. 1.1.1, it is a consequence of correlation of pairs of like nucleons moving in

⁹Within this context, and referring to one-particle transfer reactions for concreteness, the prescription of using the ratio of the absolute experimental cross section and the theoretical one – calculated in the Distorted Wave Born Approximation (DWBA) making use of Saxon-Woods single-particle wavefunctions as formfactors– to extract the single-particle content of the orbital under study (see e.g. Schiffer, J. P. et al. (2012)), may not be appropriate.

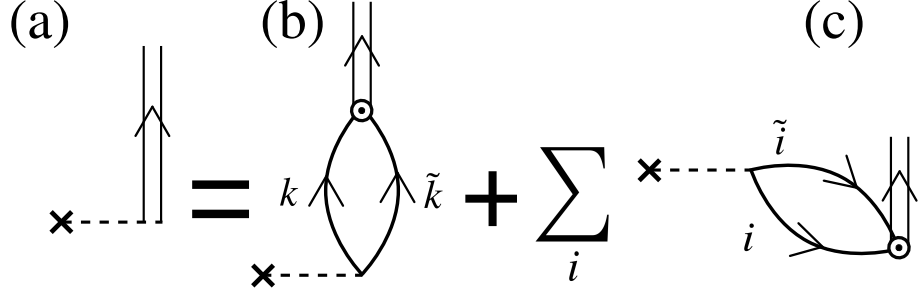


Figure 1.3.1: Graphical representation of the RPA dispersion relation describing the pair addition pairing vibrational mode, represented by a double arrowed line. Making use of the unitary transformation (1.3.6), a cross followed by a dashed horizontal line stands for: (a) the collective operator Γ_α^\dagger , (b) the operator Γ_k^\dagger creating a pair of nucleons moving in time reversal states associated with ground state correlations (k, \tilde{k}) above the Fermi energy ($\epsilon_k > \epsilon_F$); (c) The operator Γ_i^\dagger filling a pair of time reversal holes associated with ground state correlations ($\epsilon_i \leq \epsilon_F$).

time reversal states. A similar phenomenon to that found in metals at low temperatures and giving rise to superconductivity. The pairing interaction ($i = p$) can be written, within the approximation (1.3.2) used in the case of the quadrupole-quadrupole force, as

$$H_P = -P^\dagger P, \quad (1.3.4)$$

where

$$P^\dagger = \sum_{\nu>0} a_\nu^\dagger a_{\bar{\nu}}^\dagger. \quad (1.3.5)$$

Consequently, in this case the concept of independent particle field \hat{Q} (see also (1.2.4)) associated with particle-hole (ph) excitations and carrying transfer quantum number $\beta = 0$ has to be generalized to include fields describing independent pair motion, in which case $\alpha \equiv (\beta = +2, J^\pi = 0^+)$

$$\Gamma_\alpha^\dagger = \sum_k X_{kk}^\alpha \Gamma_k^\dagger + \sum_i Y_{ii}^\alpha \Gamma_i^\dagger \quad (1.3.6)$$

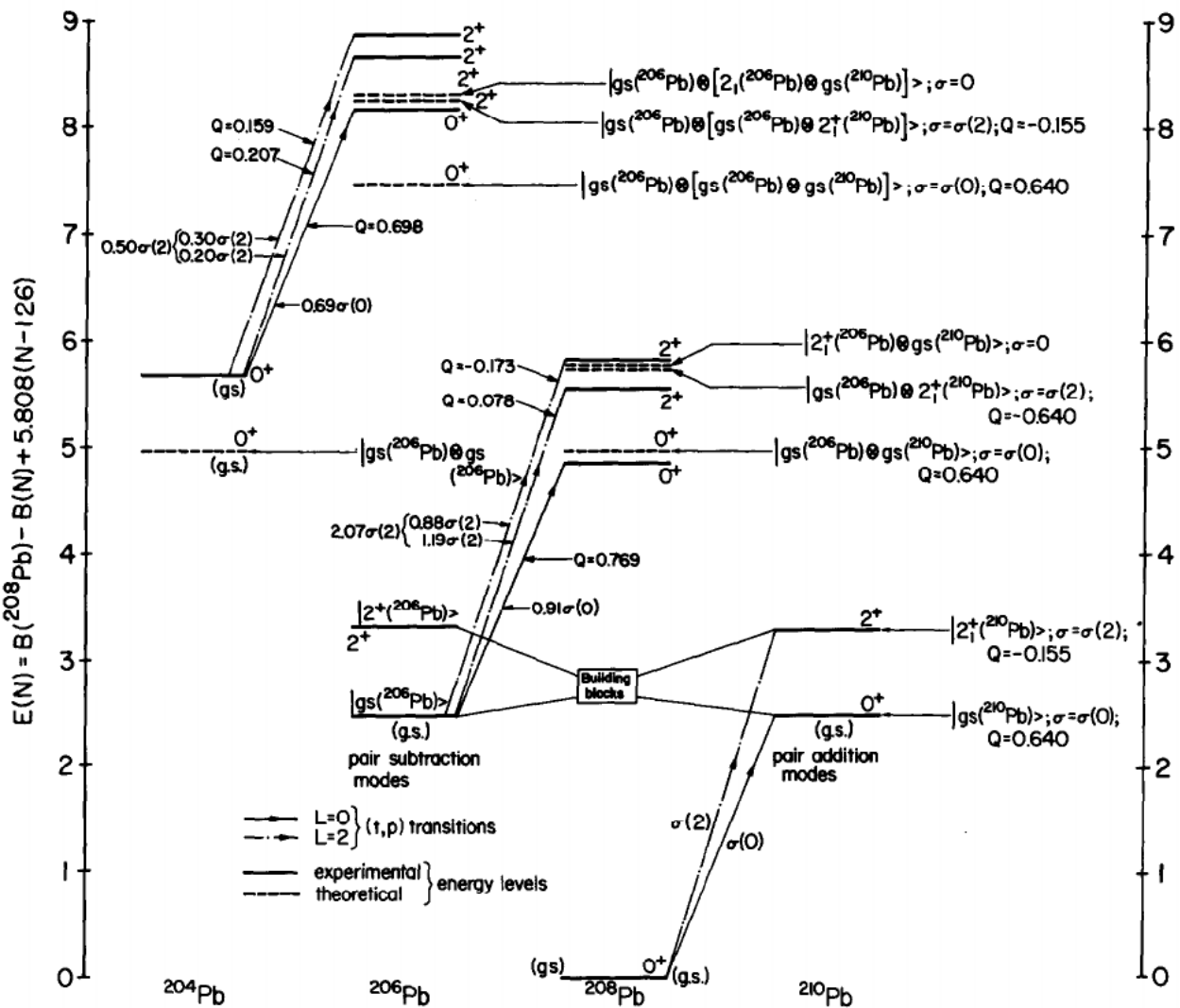
with

$$\Gamma_k^\dagger = a_k^\dagger a_{\bar{k}}^\dagger \quad (\epsilon_k > \epsilon_F), \quad \Gamma_i^\dagger = a_i^\dagger a_{\bar{i}}^\dagger \quad (\epsilon_i \leq \epsilon_F), \quad (1.3.7)$$

and

$$\sum_k X_{kk}^{\alpha 2} - \sum_i Y_{ii}^{\alpha 2} = 1, \quad (1.3.8)$$

for the pair addition ($(pp), \beta = +2$) mode, and a similar expression for the pair removal ($(hh), \beta = -2$) mode. In Fig. 1.3.1 the NFT graphical representation of the



Theoretical predictions of the pairing vibrational model for the $J^\pi = 0^+$ and 2^+ excited states of ^{208}Pb and ^{206}Pb expected to display the same Q -value, angular distribution and intensities in the $^{206}, ^{204}\text{Pb}$ (t, p) reactions as the ground state and first excited 2^+ state of ^{210}Pb in the ^{208}Pb (t, p) ^{210}Pb reaction.

These levels are depicted as dotted lines and their structure in terms of the pair addition and pair subtraction phonons (building blocks) are explicitly given.

The corresponding cross section and Q -values expected for each transition are also quoted for each state. The experimental energies (solid lines) and (t, p) cross sections are also given. In this case, the levels are joined by a continuous line ($L = 0$ transitions) or by a dotted line ($L = 2$ transitions) and the corresponding intensities in terms of the cross sections $\sigma(0) = \sigma(^{208}\text{Pb} (t, p) ^{210}\text{Pb} (\text{gs}))$ and $\sigma(2) = \sigma(^{208}\text{Pb} (t, p) ^{210}\text{Pb} (2^+))$ are given. Also quoted are the observed Q -values.

The experimental energy of the different ground states is given relative to the ^{208}Pb ground state and corrected by a linear function of the number of neutrons outside (or missing from) the $N = 126$ closed shell such that $E(^{206}\text{Pb} (\text{gs})) = E(^{210}\text{Pb} (\text{gs}))$. The corresponding expression [6] is $E_{\text{exp}}(N, Z = 82) = B(^{208}\text{Pb}) - B(N, Z = 82) + 5.808(N-126)$, where $B(N, Z)$ is the binding energy of the nucleus $A \approx N + Z$. Note that $\hbar\omega(0) = E_{\text{theor}}(^{206}\text{Pb} (\text{gs})) = E_{\text{theor}}(^{210}\text{Pb} (\text{gs})) = E_{\text{exp}}(^{206}\text{Pb} (\text{gs})) = E_{\text{exp}}(^{210}\text{Pb} (\text{gs})) = 2.493$ MeV, that $E_{\text{theor}}(^{206}\text{Pb} (2^+)) = E_{\text{exp}}(^{206}\text{Pb} (2^+)) = 3.294$ MeV and $E_{\text{theor}}(^{210}\text{Pb} (2^+)) = E_{\text{exp}}(^{210}\text{Pb} (2^+)) = 3.288$ MeV. The theoretical energy of any other state, for example of the 2^+ state $|gs(^{206}\text{Pb}) \otimes 2(^{210}\text{Pb}); 2^+\rangle$ of ^{206}Pb is equal to $2.493 + 3.294 + 2.493 = 8.280$ MeV (as measured from $^{208}\text{Pb} (\text{gs})$).

Figure 1.3.2: (After Flynn, E. R. et al. (1972)).

RPA equations for the pair addition mode is given. The state $\Gamma_\alpha^\dagger(\beta = +2)|\tilde{0}\rangle$, where $|\tilde{0}\rangle$ is the correlated ground state of a closed shell nucleus, can be viewed as the nuclear embodiment of a Cooper pair found at the basis of the microscopic theory of superconductivity.

While surface vibrations are associated with the normal ($\beta = 0$) nuclear density, pairing vibrations are connected with the so called abnormal ($\beta = \pm 2$) nuclear density (density of Cooper pairs), both static and dynamic.

Similar to the quadrupole and octupole vibrational bands built out of n_α phonons of quantum numbers $\alpha \equiv (\beta = 0, \lambda^\pi = 2^+, 3^-)$ schematically shown in Fig. 1.1.4 and experimentally observed in inelastic and Coulomb excitation and associated γ -decay processes, pairing vibrational bands build of n_α phonons of quantum numbers $\alpha \equiv (\beta = \pm 2, \lambda^\pi = 0^+, 2^+)$ have been identified around closed shells in terms of two-nucleon transfer reactions throughout the mass table (see e.g. Fig. 1.3.2).

1.4 Spontaneous broken symmetry

Because empty space is homogeneous and isotropic, the nuclear Hamiltonian is translational and rotational invariant. It also conserves particle number and is thus gauge invariant. According to quantum mechanics, the corresponding wavefunctions transform in an irreducible way under the corresponding groups of transformation. When the solution of the Hamiltonian does not have some of these symmetries, for example defines a privileged direction in space violating rotational invariance, one is confronted with the phenomenon of spontaneous broken symmetry. Strictly speaking, this can take place only for idealized systems that are infinitely large. But when one sees similar phenomena in atomic nuclei, although not so clear or regular, one recognizes that this system is after all a finite quantum many-body system (FQMBS).

1.4.1 Quadrupole deformations in 3D-space

A nuclear embodiment of the spontaneous symmetry breaking phenomenon is provided by a quadrupole deformed mean field. A situation one is confronted with, when the value of the lowest quadrupole frequency ω_2 of the RPA solution (1.1.15) tends to zero ($C_2 \rightarrow 0, D_2$ finite). A phenomenon resulting from the interplay of the interaction v (H_{QQ} in (1.3.2)), and of the nucleons outside closed shell, leading to tidal-like polarization of the spherical core.

Coordinate and linear momentum ((x, p_x) single-particle motion) as well as Euler angles and angular momentum ((φ, I_z) rotational in two-dimensional (2D)-space) are conjugate variables. Similarly, the gauge angle and the number of particles ((ϕ, N) rotation in gauge space), fulfill $[\phi, N] = i$. The operators $e^{-ip_x x}$, $e^{-i\varphi I_z}$ and $e^{-iN\phi}$ induce Galilean transformation and rotations in 2D- and in gauge space respectively.

Making again use, for didactical purposes, of H_{QQ} instead of v , and calling $|N\rangle$

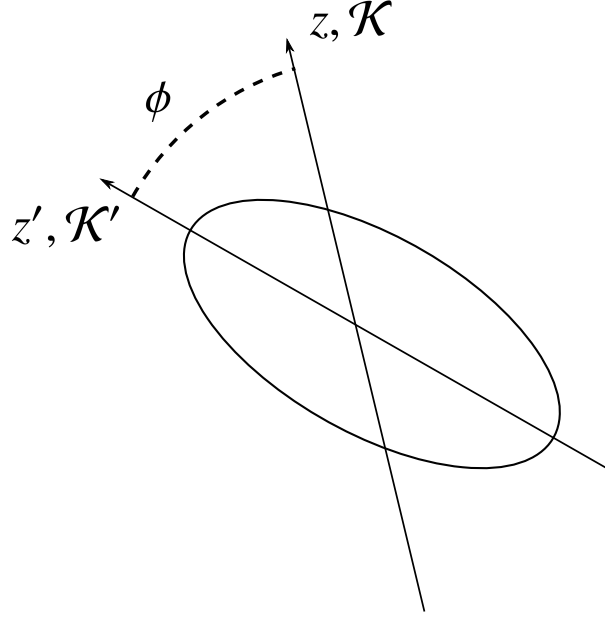


Figure 1.4.1: Schematic representation of deformation in gauge space, where the laboratory (\mathcal{K}) and the intrinsic (\mathcal{K}' , body fixed) frames of reference are also indicated.

the eventual mean field solution of the Hamiltonian $T + H_{QQ}$, one expects

$$\langle N | \hat{Q} | N \rangle = Q_0, \quad (1.4.1)$$

where, for simplicity, we assumed axial symmetry ($\lambda = 2, \mu = 0$). That is, the emergence of a static quadrupole deformation. Rewriting H_{QQ} in terms of $(\hat{Q}^\dagger - Q_0 + Q_0)$ and its Hermitian conjugate, one obtains

$$H = H_{sp} + H_{QQ} = H_{MF} + H_{fluct}, \quad (1.4.2)$$

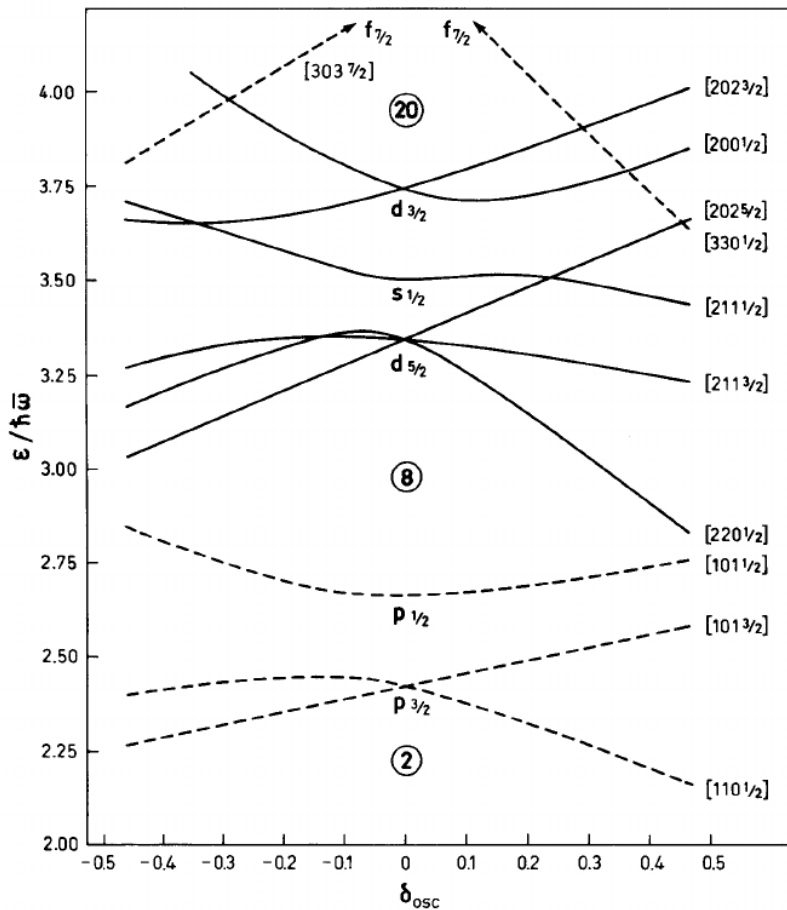
where

$$H_{MF} = H_{sp} - \kappa(\hat{Q}^\dagger + \hat{Q}), \quad (1.4.3)$$

is the mean field, and

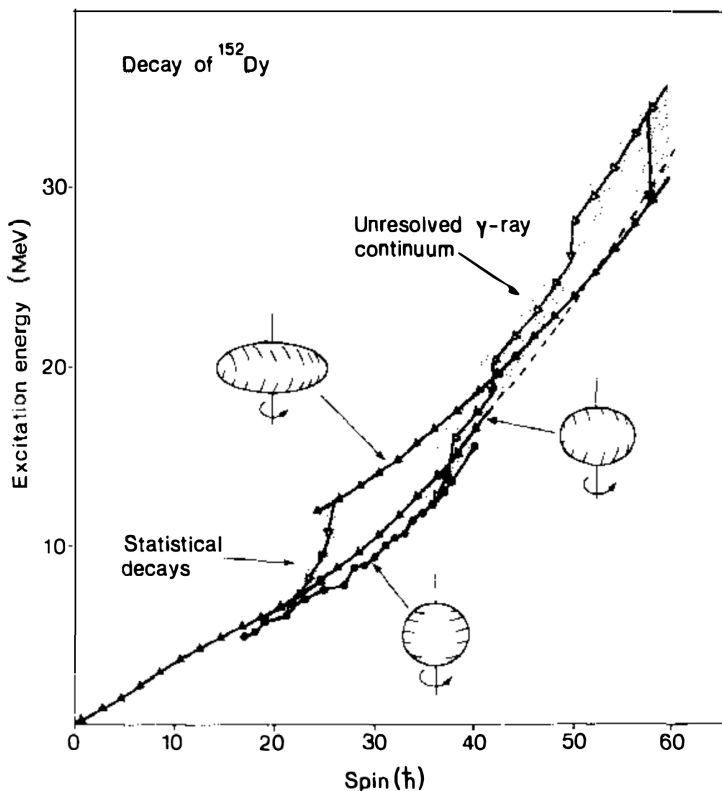
$$H_{fluct} = -\kappa(\hat{Q}^\dagger - Q_0)(\hat{Q} - Q_0) \quad (1.4.4)$$

the residual interaction inducing fluctuations around Q_0 . Assuming $Q_0 \gg (\hat{Q}^\dagger - Q_0)(\hat{Q} - Q_0)$, we concentrate on H_{MF} . The original realization of it is known as the Nilsson Hamiltonian (Nilsson (1955)). It describes the motion of nucleons in a single-particle potential of radius $R_0(1 + \beta_2 Y_{20}(\hat{r}))$, with β_2 proportional to the intrinsic quadrupole moment Q_0 ($\beta_2 \approx Q_0/(ZR_0^2)$). The reflection invariance and



Spectrum of single-particle orbits in spheroidal potential (N and $Z < 20$). The spectrum is taken from B. R. Mottelson and S. G. Nilsson, *Mat. Fys. Skr. Dan. Vid. Selsk.* **1**, no. 8 (1959). The orbits are labeled by the asymptotic quantum numbers $[Nn_l\Lambda\Omega]$ referring to large prolate deformations. Levels with even and odd parity are drawn with solid and dashed lines, respectively.

Figure 1.4.2: (After Bohr, A. and Mottelson (1975)).



A schematic of the proposed γ -ray decay paths from a high-spin entry point in ^{152}Dy . The major initial decay flow occurs mainly via E2 transitions in the unresolved γ -ray continuum and reaches the oblate yrast structures between $30\hbar$ and $40\hbar$. A small 1% branch feeds the superdeformed band, which is assumed to become yrast at a spin of $50\hbar$ – $55\hbar$. The deexcitation of the superdeformed band around $26\hbar$ occurs when the band is 3–5 MeV above yrast, and a statistical type of decay flow takes it into the oblate states between $19\hbar$ and $25\hbar$.

Figure 1.4.3: (After Nolan and Twin (1988)).

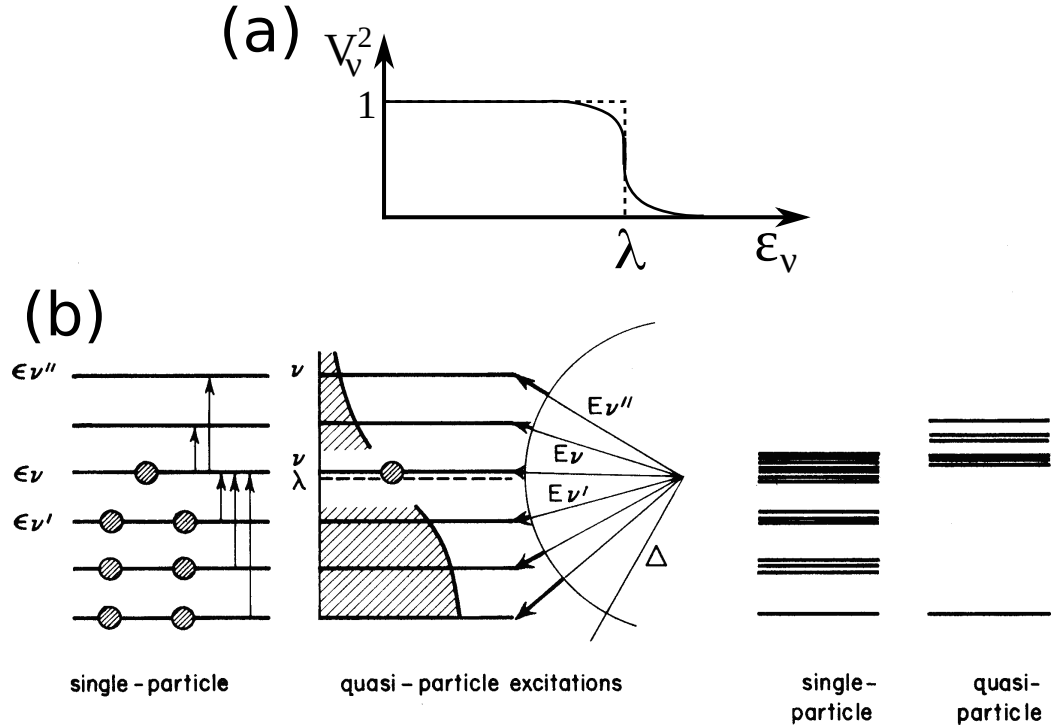


Figure 1.4.4: (a) Independent (dashed line) and BCS occupation numbers; (b) ground state and excited states in the extreme single-particle model and in the pairing-correlated, superfluid model in the case of a system with an odd number of particles. In the first case, the energy of the ground state of the odd system differs from that of the even with one particle fewer by the energy difference $\epsilon_v - \epsilon_{v'}$, while in the second case by the energy $E_v = \sqrt{(\epsilon_v - \lambda)^2 + \Delta^2} \approx \Delta$, associated with the fact the odd particle has no partner. Excited states can be obtained in the independent particle case, where it is assumed that levels are two-fold degenerate (Kramers degeneracy) by promoting the odd particle to states above the level ϵ_v , or one particle to states above ν' (arrows). To the left only a selected number of these excitations are shown. In the superfluid case excited states can be obtained by breaking of pairs in any orbit. The associated quasiparticle energy is drawn also here by an arrow of which the thin part indicates the contribution of the pairing gap and the thick part indicates the kinetic energy contribution, i.e. the contribution arising from the single-particle motion. Note the very different density of levels emerging from these two pictures, which are shown at the far right of the figure (after Nathan and Nilsson (1965)).

axial symmetry of the Nilsson Hamiltonian implies that parity π and projection Ω of the total angular momentum along the symmetry axis are constants of motion for the one-particle Nilsson states. These states, are two-fold degenerate, since two orbits that differ only in the sign of Ω represent the same motion, apart from the clockwise and anticlockwise sense of revolution around the symmetry axis. One can thus write the Nilsson creation operators in terms of a linear combination of creation operators carrying good total angular momentum j ,

$$\gamma_{a\Omega}^\dagger = \sum_j A_j^a a_{aj\Omega}^\dagger, \quad (1.4.5)$$

where the label a stands for all the quantum numbers aside from Ω , which specify the orbital.

Expressed in the intrinsic, body-fixed, system of coordinates \mathcal{K}' (Fig. 1.4.1) where the 3 (z') axis lies along the symmetry axis and the 1 and 2 (x', y') axis lie in a plane perpendicular to it, namely

$$\gamma'_{a\Omega}^\dagger = \sum_j A_j^a \sum_{\Omega'} \mathcal{D}_{\Omega\Omega'}^2(\omega) a_{aj\Omega'}^\dagger, \quad (1.4.6)$$

one can write the Nilsson state as

$$|N(\omega)\rangle_{\mathcal{K}'} = \prod_{a\Omega>0} \gamma_{a\Omega}^\dagger \gamma'_{a\Omega}^\dagger |0\rangle_F, \quad (1.4.7)$$

where ω represent the Euler angles, $|0\rangle_F$ is the particle vacuum, and $|a\tilde{\Omega}\rangle = \gamma_{a\tilde{\Omega}}^\dagger |0\rangle_F$ is the state time-reversed to $|a\Omega\rangle$. For well deformed nuclei, a conventional description of the one-particle motion is based on the similarity of the nuclear potential to that of an anisotropic nuclear potential,

$$V = \frac{1}{2} M \left(\omega_3^2 x_3^2 + \omega_\perp^2 (x_1^2 + x_2^2) \right) = \frac{1}{2} M \omega_0 r^2 \left(1 - \frac{4}{3} \delta P_2(\cos \theta) \right), \quad (1.4.8)$$

with $\omega_3 \omega_\perp^2 = \omega_0^3$. That is a volume which is independent of the deformation $\delta \approx 0.95\beta_2$. The corresponding single-particle states have energy

$$\epsilon(n_3 n_\perp) = (n_3 + \frac{1}{2})\hbar\omega_3 + (n_\perp + \frac{1}{2})\hbar\omega_\perp, \quad (1.4.9)$$

where n_3 and $n_\perp = n_1 + n_2$ are the number of quanta along and perpendicular to the symmetry axis. The degenerate states with the same value of n_\perp can be specified by the component Λ of the orbital angular momentum along the symmetry axis,

$$\Lambda = \pm n_\perp, \pm(n_\perp - 2), \dots, \pm 1 \text{ or } 0. \quad (1.4.10)$$

One can then label the Nilsson levels in terms of the asymptotic quantum numbers $[N n_3 \Lambda \Omega]$, where $N = n_3 + n_\perp$, is the total oscillator quantum number. The complete expression of the Nilsson potential includes, aside from the central term discussed

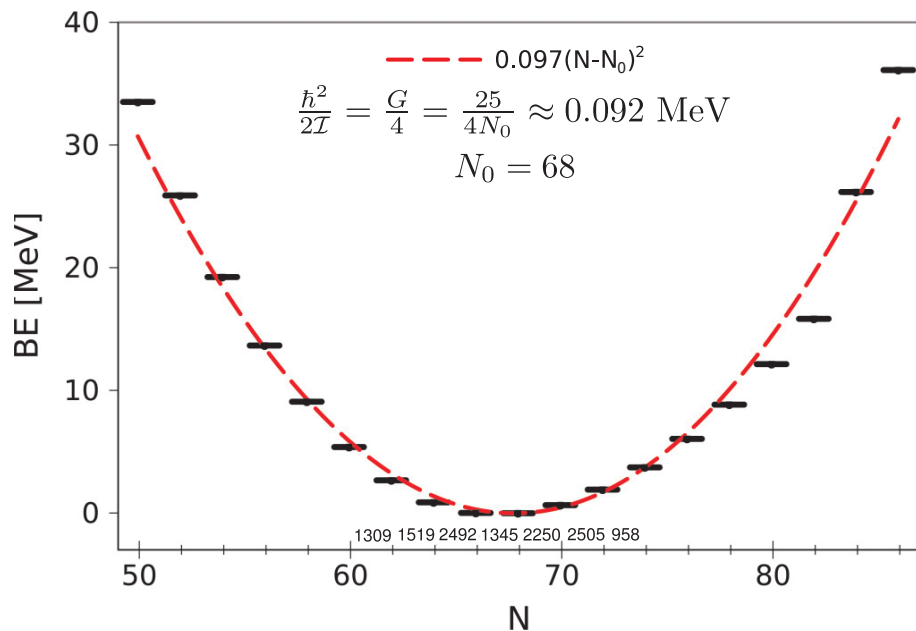


Figure 1.4.5: Pairing rotational band associated with the ground states of the Sn-isotopes. The lines represent the energies calculated according to the expression $BE = B(^{50+N}\text{Sn}_N) - 8.124N + 46.33$ (Brink, D. and Broglia (2005)), subtracting the contribution of the single nucleon addition to the nuclear binding energy obtained by a linear fitting of the binding energies of the whole Sn chain. The estimate of $\hbar^2/2I$ was obtained using the single j -shell model (see, e.g., Brink, D. and Broglia (2005), Appendix H). The numbers given on the abscissa are the absolute value of the experimental $gs \rightarrow gs$ cross section (in units of μb). (After Potel, G. et al. (2013)).

above, a spin-orbit and a term proportional to the orbital angular momentum quantity squared, so as to make the shape of the oscillator to resemble more that of a Saxon-Woods potential. The resulting levels provide an overall account of the experimental findings, providing detailed evidence in terms of individual states of the interplay between the single-particle and the collective aspects of nuclear structure. An example of relevance for light nuclei (N and $Z < 20$) is given in Fig. 1.4.2.

The Nilsson intrinsic state (1.4.7) does not have a definite angular momentum but is rather a superposition of such states,

$$|N(\omega)\rangle_{\mathcal{K}'} = \sum C_I |I\rangle. \quad (1.4.11)$$

Because there is no restoring force associated with different orientations of $|N(\omega)\rangle_{\mathcal{K}'}$, fluctuations in the Euler angle diverge in the right way to restore rotational invariance, leading to a rotational band whose members are

$$|IKM\rangle \sim \int d\omega \mathcal{D}_{MK}^I(\omega) |N(\omega)\rangle_{\mathcal{K}'}, \quad (1.4.12)$$

with energy

$$E_I = \frac{\hbar^2}{2I} I(I+1). \quad (1.4.13)$$

The quantum numbers I, M, K are the total angular momentum I , and its third component M and K along the laboratory (z) and intrinsic (z') frame references respectively. Rotational bands have been observed up to rather high angular momenta in terms of individual transitions. An example extending up to $I = 60\hbar$ is given in Fig. 1.4.3.

1.4.2 Deformation in gauge space

Let us now turn to the pairing Hamiltonian. In the case in which $\hbar\omega_{\beta=-2} = \hbar\omega_{\beta=2} = 0$, the system deforms, this time in gauge space. Calling $|BCS\rangle$ the mean field solution of the pairing Hamiltonian, leads to the finite expectation value

$$\alpha_0 = \langle BCS | P^\dagger | BCS \rangle, \quad (1.4.14)$$

of the pair creation operator P^\dagger , quantity which can be viewed as the order parameter of the new deformed phase of the system in gauge space. The total Hamiltonian can be written as

$$H = H_{MF} + H_{fluct}, \quad (1.4.15)$$

where

$$H_{MF} = H_{sp} - \Delta(P^\dagger + P) + \frac{\Delta^2}{G} \quad (1.4.16)$$

and

$$H_{fluct} = -G(P^\dagger - \alpha_0)(P - \alpha_0). \quad (1.4.17)$$

The quantity

$$\Delta = G\alpha_0, \quad (1.4.18)$$

is the so called pairing gap (Fig. 1.4.4), which measures the binding energy of Cooper pairs, the quantity α_0 being the number of Cooper pairs.

The mean field pairing Hamiltonian

$$H_{MF} = \sum_{\nu>0} (\epsilon_\nu - \lambda) (a_\nu^\dagger a_\nu + a_{\tilde{\nu}}^\dagger a_{\tilde{\nu}}) - \Delta \sum_{\nu>0} (\epsilon_\nu - \lambda) (a_\nu^\dagger a_{\tilde{\nu}}^\dagger + a_{\tilde{\nu}} a_\nu) + \frac{\Delta^2}{G} \quad (1.4.19)$$

is a bilinear expression in the creation and annihilation operator, ν labeling the quantum numbers of the single-particle orbitals where nucleons are allowed to correlate e.g. $(nljm)$ while $\tilde{\nu}$ denotes the time reversal state which in this case is degenerate with ν and has quantum numbers $(nlj - m)$, $\nu > 0$ implying that one sums over $m > 0$. It is of notice that

$$\hat{N} = \sum_{\nu>0} (a_\nu^\dagger a_\nu + a_{\tilde{\nu}}^\dagger a_{\tilde{\nu}}), \quad (1.4.20)$$

is the number operator, and $\lambda \hat{N}$ in Eq. (1.4.19) acts as the Coriolis force in the body-fixed frame of reference in gauge space.

One can diagonalize H_{MF} by a rotation in the (a^\dagger, a) -space. This can be accomplished through the Bogoliubov-Valatin transformation

$$\alpha_\nu^\dagger = U_\nu a_\nu^\dagger - V_\nu a_{\tilde{\nu}}, \quad (1.4.21)$$

The BCS solution does not change the energies ϵ_ν (measured in (1.4.19) from the Fermi energy λ) of the single-particle levels or associated wavefunctions $\varphi_\nu(\mathbf{r})$, but the occupation probabilities for levels around the Fermi energy within an energy range 2Δ ($2\Delta/\lambda \approx 2 \text{ MeV}/36 \text{ MeV} \approx 0.06$). The quasiparticle operator α_ν^\dagger creates a particle in the single-particle state ν with probability U_ν^2 , while it creates a hole (annihilates a particle) with probability V_ν^2 . To be able to create a particle, the state ν should be empty, while to annihilate a particle it has to be filled, so U_ν^2 and V_ν^2 are the probabilities that the state ν is empty and is occupied respectively. Within this context, the one quasiparticle states

$$|\nu\rangle = \alpha_\nu^\dagger |BCS\rangle \quad (1.4.22)$$

are orthonormal. In particular

$$\langle \nu | \nu \rangle = 1 = \langle BCS | \alpha_\nu \alpha_\nu^\dagger | BCS \rangle = \langle BCS | \{\alpha_\nu, \alpha_\nu^\dagger\} | BCS \rangle = U_\nu^2 + V_\nu^2, \quad (1.4.23)$$

where the relations

$$\{a_\nu, a_{\nu'}^\dagger\} = \delta(\nu, \nu') \quad (1.4.24)$$

and

$$\{a_\nu, a_{\nu'}\} = \{a_\nu^\dagger, a_{\nu'}^\dagger\} = 0 \quad (1.4.25)$$

have been used. Note that the $|BCS\rangle$ state is the quasiparticle vacuum

$$\alpha_\nu |BCS\rangle = 0, \quad (1.4.26)$$

in a similar way in which $|0\rangle_F$ is the particle vacuum. Inverting the quasiparticle transformation (1.4.21) and its complex conjugate, i.e. expressing a_ν^\dagger and a_ν (and time reversals (tr)) in terms of α_ν^\dagger and α_ν (and tr) one can rewrite (1.4.19) in terms of quasiparticles.

Minimizing the energy $E_0 = \langle BCS|H|BCS\rangle$ in terms of V_ν

$$\frac{\partial E_0}{\partial V_\nu} = 0 \quad (1.4.27)$$

and making use of the expression for the average of particles

$$N_0 = \langle BCS|\hat{N}|BCS\rangle = 2 \sum_{\nu>0} V_\nu^2, \quad (1.4.28)$$

and of the number of Cooper pairs

$$\alpha_0 = \langle BCS|P^\dagger|BCS\rangle = \sum_{\nu>0} U_\nu V_\nu \quad (1.4.29)$$

and of the pairing gap

$$\Delta = G \sum_{\nu>0} U_\nu V_\nu, \quad (1.4.30)$$

one obtains,

$$H_{MF} = H_{11} + U \quad (1.4.31)$$

where

$$H_{11} = \sum_\nu E_\nu \alpha_\nu^\dagger \alpha_\nu \quad (1.4.32)$$

and

$$U = 2 \sum_{\nu>0} (\epsilon_\nu - \lambda) V_\nu^2 - \frac{\Delta^2}{G}. \quad (1.4.33)$$

The quantity

$$E_\nu = \sqrt{(\epsilon_\nu - \lambda)^2 + \Delta^2} \quad (1.4.34)$$

is the quasiparticle energy, while the probability amplitudes are

$$V_\nu = \frac{1}{\sqrt{2}} \left(1 - \frac{\epsilon_\nu - \lambda}{E_\nu} \right)^{1/2} \quad (1.4.35)$$

$$U_\nu = \frac{1}{\sqrt{2}} \left(1 + \frac{\epsilon_\nu - \lambda}{E_\nu} \right)^{1/2} \quad (1.4.36)$$

From the relations (1.4.28) and (1.4.30) one obtains

$$N_0 = 2 \sum_{\nu>0} V_\nu^2 \quad (1.4.37)$$

and

$$\frac{1}{G} = \sum_{\nu>0} \frac{1}{2E_\nu}. \quad (1.4.38)$$

These equations allow one to calculate the parameters λ and Δ from the knowledge of G and ϵ_ν , parameters which completely determine E_ν , V_ν and U_ν and thus the BCS mean field solution (Fig. 1.4.4). The validity of the BCS description of superfluid open shell nuclei have been confirmed throughout the mass table. We provide below recent examples.

The relation (1.4.26) implies that

$$\begin{aligned} |BCS\rangle &= \frac{1}{\text{Norm}} \prod_{\nu>0} \alpha_\nu \alpha_{\tilde{\nu}} |0\rangle_F = \prod_{\nu>0} (U_\nu + V_\nu P_\nu^\dagger) |0\rangle_F \\ &= \left(\prod_{\nu>0} U_\nu \right) \sum_{N \text{ even}} \frac{(c_\nu P_\nu^\dagger)^{N/2}}{(N/2)!} |0\rangle_F, \end{aligned} \quad (1.4.39)$$

where

$$P_\nu^\dagger = a_\nu^\dagger a_{\tilde{\nu}}^\dagger \quad \left(P^\dagger = \sum_{\nu>0} P_\nu^\dagger \right), \quad c_\nu = V_\nu / U_\nu. \quad (1.4.40)$$

In the above discussion of BCS we have treated in a rather cavalier fashion the fact that the amplitudes U_ν and V_ν are in fact complex quantities. A possible choice of phasing is¹⁰

$$U_\nu = U'_\nu; \quad V_\nu = V'_\nu e^{-2i\phi}, \quad (1.4.41)$$

¹⁰The same results as those which will be derived are obtained with the alternative choice $U_\nu = U'_\nu e^{i\phi}$, $V_\nu = V'_\nu e^{-i\phi}$.

U'_ν and V'_ν being real quantities, while ϕ is the gauge angle, conjugate variable to the number of particles operator (1.4.20). Then¹¹

$$\hat{\phi} = i\partial/\partial\mathcal{N}, \quad \mathcal{N} \quad (1.4.42)$$

and

$$[\hat{\phi}, \mathcal{N}] = i \quad (1.4.43)$$

where $\mathcal{N} \equiv \hat{N}$ (Eq. (1.4.20)), gauge transformations being induced by the operator

$$\mathcal{G}(\phi) = e^{-i\mathcal{N}\phi}. \quad (1.4.44)$$

Let us introduce the amplitudes (1.4.41) in (1.4.23)

$$|BCS\rangle = \left(\prod_{\nu>0} U'_\nu \right) \sum_{N \text{ even}} e^{-iN\phi} |\Phi_N\rangle = \left(\prod_{\nu>0} U'_\nu \right) \sum_{N \text{ even}} e^{-iN\phi} |\Phi_N\rangle \quad (1.4.45)$$

where

$$|\Phi_N\rangle = \frac{\left(\sum_{\nu>0} c'_\nu P_\nu^\dagger \right)^{N/2}}{(N/2)!} |0\rangle_F, \quad (1.4.46)$$

with $c'_\nu = V'_\nu/U'_\nu$. It is of notice that

$$\sum_{\nu>0} c'_\nu P_\nu^\dagger |0\rangle_F \quad (1.4.47)$$

is the single Cooper pair state. The $|BCS\rangle$ state does not have a definite number of particles, but only in average being a wavepacket in N .

In fact, (1.4.44) defines a privileged direction in gauge space, being an eigenstate of $\hat{\phi}$

$$\hat{\phi}|BCS\rangle = i \frac{\partial}{\partial\mathcal{N}} \left(\prod_{\nu>0} U'_\nu \right) \sum_{N \text{ even}} e^{-iN\phi} |\Phi_N\rangle = \phi |BCS\rangle. \quad (1.4.48)$$

Expressing it differently (1.4.44) can be viewed as an axially symmetric deformed system in gauge space, whose symmetry axis coincides with the z' component of the body-fixed frame of reference \mathcal{K}' , which makes an angle ϕ with the laboratory z -axis (Fig. 1.4.1).

With the help of Eq. (1.4.39) (first line) one can write

$$|BCS(\phi=0)\rangle_{\mathcal{K}'} = \prod_{\nu>0} (U'_\nu + V'_\nu P_\nu^\dagger) |0\rangle_F, \quad (1.4.49)$$

¹¹See e.g. Brink, D. and Broglia (2005) App. H and refs. therein.

where use was made of the relations

$$\mathcal{G}(\phi) a_\nu^\dagger \mathcal{G}^{-1}(\phi) = e^{-i\phi} a_\nu^\dagger = a_\nu'^\dagger, \quad (1.4.50)$$

and

$$\mathcal{G}(\phi) P_\nu^\dagger \mathcal{G}^{-1}(\phi) = e^{-2i\phi} P_\nu^\dagger = P_\nu'^\dagger. \quad (1.4.51)$$

It is to be noted that \mathcal{G} induces a counter clockwise rotation,

$$\mathcal{G}(\chi) \hat{\phi} \mathcal{G}^{-1}(\chi) = \hat{\phi} - \chi. \quad (1.4.52)$$

As a consequence, to rotate $|BCS(\phi = 0)\rangle_{\mathcal{K}'}$ back into the laboratory system, use has to be made of the clockwise rotation of angle ϕ induced by $\mathcal{G}^{-1}(\phi)$,

$$\begin{aligned} \mathcal{G}^{-1}(\phi) |BCS(\phi = 0)\rangle_{\mathcal{K}'} &= \prod_{\nu>0} (U'_\nu + V'_\nu \mathcal{G}^{-1}(\phi) P_\nu'^\dagger) |0\rangle_F \\ &= \prod_{\nu>0} (U'_\nu + e^{2i\phi} V_\nu P_\nu^\dagger) |0\rangle_F = |BCS(\phi)\rangle_{\mathcal{K}} \end{aligned} \quad (1.4.53)$$

where use was made of (1.4.49)

$$\mathcal{G}^{-1}(\phi) (\mathcal{G}(\phi) P_\nu^\dagger \mathcal{G}^{-1}(\phi)) \mathcal{G}(\phi) = \mathcal{G}^{-1}(\phi) P_\nu'^\dagger \mathcal{G}(\phi). \quad (1.4.54)$$

We note furthermore

$$|BCS(\phi = 0)\rangle_{\mathcal{K}'} = \prod_{\nu>0} (U'_\nu + V'_\nu P_\nu'^\dagger) |0\rangle_F = \prod_{\nu>0} (U_\nu + V_\nu P_\nu^\dagger) |0\rangle_F. \quad (1.4.55)$$

Spontaneous broken symmetry in nuclei is, as a rule associated with the presence of rotational bands, as already found in the case of quadrupole deformed nuclei. Consequently, one expects in nuclei with $\Delta \neq 0$ rotational bands in which particle number plays the role of angular momentum. That is pairing rotational bands.

In what follows we will discuss the structure of H_{fluct} and single out the term responsible for restoring gauge invariance to the BCS mean field solution giving thus, rise to pairing rotational bands. In terms of quasiparticles, H_{fluct} can be expressed as

$$H_{fluct} = H'_p + H''_p + C \quad (1.4.56)$$

where

$$H'_p = -\frac{G}{4} \left(\sum_{\nu>0} (U_\nu^2 - V_\nu^2) (\Gamma_\nu^\dagger + \Gamma_\nu) \right)^2 \quad (1.4.57)$$

and

$$H''_p = \frac{G}{4} \left(\sum_{\nu} (\Gamma_\nu^\dagger - \Gamma_\nu) \right)^2, \quad (1.4.58)$$

with

$$\Gamma_\nu^\dagger = \alpha_\nu^\dagger \alpha_{\bar{\nu}}^\dagger. \quad (1.4.59)$$

The term C stands for constant terms, as well as for terms proportional to the number of quasiparticles, which consequently vanish when acting on $|BCS\rangle$. The term H'_p gives rise to two-quasiparticle pairing vibrations with energies $\gtrsim 2\Delta$. It can be shown that it is the term H''_p which restores gauge invariance¹²,

$$[H_{MF} + H''_p, \hat{N}] = 0 \quad (1.4.60)$$

We now diagonalize $H_{MF} + H''_p$ in the quasiparticle RPA (QRPA),

$$[H_{MF} + H''_p, \Gamma_n^\dagger] = \hbar\omega_n \Gamma_n^\dagger, \quad [\Gamma_n, \Gamma_{n'}^\dagger] = \delta(n, n'), \quad (1.4.61)$$

where

$$\Gamma_n^\dagger = \sum_\nu (a_{n\nu} \Gamma_\nu^\dagger + b_{n\nu} \Gamma_\nu), \quad \Gamma_\nu^\dagger = \alpha_\nu^\dagger \alpha_{\bar{\nu}}^\dagger, \quad (1.4.62)$$

is the creation operator of the n th vibrational mode. In the case of the $n = 1$, lowest energy root, it can be written as

$$|1''\rangle = \Gamma_1^{\prime\dagger} |0''\rangle = \frac{\Lambda_1''}{2\Delta} (\hat{N} - N_0) |0''\rangle, \quad (1.4.63)$$

where \hat{N} is the particle number operator written in terms of Γ_ν^\dagger and Γ_ν , and Λ_1'' is the strength of the quasiparticle-mode coupling. The prefactor is the zero point fluctuation (ZPF) of the mode, that is (see Eq. (1.1.11) in the case of surface vibration),

$$\sqrt{\frac{\hbar\omega_1''}{2C_1'}} = \sqrt{\frac{\hbar^2}{2D_1''\hbar\omega_1''}}. \quad (1.4.64)$$

Because the lowest frequency is $\omega_1'' = 0$, the associated ZPF diverge ($\Lambda_1'' \sim (\hbar\omega_1'')^{-1/2}$). It can be seen that this is because $C_1'' \rightarrow 0$, while D_1'' remains finite. In fact,

$$\frac{D_1''}{\hbar^2} = \frac{2\Delta^2}{\Lambda_1''^2 \hbar\omega_1''} = 4 \sum_{\nu>0} \frac{U_\nu^2 V_\nu^2}{2E_\nu}. \quad (1.4.65)$$

A rigid rotation in gauge space can be generated by a series of infinitesimal operations of type $\mathcal{G}(\delta\phi) = e^{i(\hat{N}-N_0)\delta\phi}$, the one phonon state $|1''\rangle = \Gamma_1^{\prime\dagger} |0''\rangle$, is obtained from rotations in gauge space of divergent amplitude. That is, fluctuations of ϕ

¹²For details see Brink, D. and Broglia (2005).

over the whole $0 - 2\pi$ range. By proper inclusion of these fluctuations one can restore gauge invariance violated by $|BCS\rangle_{\mathcal{K}'}$. The resulting states

$$|N_0\rangle \sim \int_0^{2\pi} d\phi e^{-iN_0\phi} |BCS(\phi)\rangle_{\mathcal{K}'} \left(\sum_{\nu>0} c'_\nu P_\nu^\dagger \right)^{N/2} |0\rangle_F \quad (1.4.66)$$

have a definite number of particles and constitute the members of a pairing rotational band. Making use of a simplified model (single j -shell) it can be shown that the energies of those states can be written as,

$$E_N = \lambda(N - N_0) + \frac{G}{4} (N - N_0)^2, \quad (1.4.67)$$

where

$$\frac{G}{4} = \frac{\hbar^2}{2D'_1}. \quad (1.4.68)$$

An example of pairing rotational bands is provided by the ground state of the single open closed shell superfluid isotopes of the $^{50}_{50}\text{Sn}_N$ -isotopes (Fig. 1.4.5), $N_0 = 68$ having been used in the solution of the BCS number equation (1.4.37). Theory provides an overall account of the experimental findings. Making use of the BCS pair transfer amplitudes,

$$\langle BCS | P_\nu^\dagger | BCS \rangle = U_\nu V_\nu \quad (1.4.69)$$

in combination with a reaction software and of global optical parameters, one can account for the absolute value of the pair transfer differential cross section, within experimental errors (see Ch. 7 ??). The fact that projecting out the different Sn-isotopes from the intrinsic BCS state describing ^{118}Sn one obtains a quantitative description of observations carried out with the help of the specific probe of pairing correlations (Cooper pair transfer), testifies to the fact that pairing rotational bands can be considered elementary modes of nuclear excitation, emergent properties of spontaneous symmetry breaking of gauge invariance.

Furthermore, the fact that these results follow the use of QRPA¹³ in the calculation of the ZPF of the collective solutions of the pairing Hamiltonian indicates the importance of conserving approximations to describe quantum many-body problems in general, and the finite size quantum many-body problem (FSQMB), of which the nuclear case represents a paradigmatic example, in particular.

Aside from low-lying collective states, that is rotations and low-energy vibrations, nuclei also display high-lying collective modes known as giant resonances.

¹³Using the Tamm-Dancoff approximation, i.e. setting $Y \equiv 0$ (and thus $\sum X^2 = 1$) in the QRPA approximation does not lead to particle number conservation, in keeping with the fact that the amplitudes Y are closely connected with ZPF.

1.5 Giant dipole resonance

If one shines a beam of photons on a nucleus it is observed that the system absorbs energy resonantly essentially at a single frequency, of the order of¹⁴ $\nu = 5 \times 10^{21}$ Hz, corresponding to an energy of $h\nu \approx 20$ MeV.

It is not difficult to understand how γ -rays excite a nuclear dipole vibration. A photon carries with it an oscillating electric field. Although the wavelength of a 20 MeV γ -ray is smaller than that of other forms of electromagnetic radiation such as visible light, it is still large ($\lambda \approx 63$ fm) compared to the dimensions of e.g. ^{40}Ca ($R_0 \approx 4.1$ fm). As a result the photon electric field is nearly uniform across the nucleus at any time. The field exerts a force on the positively charged protons. Consequently, it can set the center of mass into an antenna like, dipole oscillation (Thompson scattering), in which case no photon is absorbed. Another possibility is that it leads to an internal excitation of the system. In this case because the center of mass of the system does not move, the neutrons have to oscillate against the protons, again in an antenna-like motion. The restoring force of the vibration, known as the giant dipole resonance (GDR), is provided by the attractive force between protons and neutrons.

The connotation of giant is in keeping with the fact that it essentially carries the full photo absorption cross section (energy weighted sum rule, see below), and resonance because it displays a Lorentzian-like shape with a full width at half maximum of few MeV ($\lesssim 5$ MeV), considerably smaller than the energy centroid¹⁵ $\hbar\omega_{GDR} \approx 80/A^{1/3}$ MeV. Microscopically, the GDR can be viewed as a correlated particle-hole excitation, that is a state made out of a linear contribution of proton and neutron particle-hole excitations with essentially $\Delta N = 1$, as well as small $\Delta N = 3, 5, \dots$ components (Fig. 1.1.3). Because the difference in energy between major shells is $\hbar\omega_0 \approx 41A^{1/3}$ MeV, one expects that about half of the contribution to the energy arises from the neutron-proton interaction. More precisely, from the so called (repulsive) symmetry potential V_1 (see Eq. (1.1.4)), which measures the energy price the system has to pay to separate protons from neutrons. Theoretical estimates lead to

$$(\hbar\omega_{GDR})^2 = (\hbar\omega_0)^2 + \frac{3\hbar^2 V_1}{m\langle r^2 \rangle} = \frac{1}{A^{2/3}} [(41)^2 + (60)^2] \text{ MeV}^2, \quad (1.5.1)$$

resulting in

¹⁴Making use of $h = 4.1357 \times 10^{-15}$ eVs one obtains for $h\nu = 1$ eV the frequency $\nu = 2.42 \times 10^{14}$ Hz and thus $\nu = 4.8 \times 10^{21}$ Hz for $h\nu = 20$ MeV. The wavelength of a photon of energy E is $\lambda = hc/E \approx 2\pi \times 200$ MeV fm/ E , which for $E = 20$ MeV leads to $\lambda \approx 63$ fm.

¹⁵Within this context we refer to the discussion concerning the renormalization of collective modes carried out in the text after equation (1.2.8), in particular regarding the cancellation between self-energy and vertex corrections (see Fig. 1.2.5 and footnote 7). This is a basic result of NFT –as discussed in later chapters– being connected with sum rule arguments in general, and particle conservation in particular. Argument which has been extended to the case of finite temperature as well as to include relativistic effects Nambu (1960); Ward (1950); Bortignon and Broglia (1981); Bertsch et al. (1983); Bortignon, P. F. et al. (1998); Litvinova and Wibowo (2018); Wibowo and Litvinova (2019).

$$\hbar\omega_{GDR} \approx \frac{73}{A^{1/3}} \approx \frac{87}{R} \text{ MeV}, \quad (1.5.2)$$

where $R = 1.2A^{1/3}$ is the numerical value of the nuclear radius measured in fm. The above quantity is to be compared with the empirical value $\hbar\omega_{GDR} \approx (80/A^{1/3})$ MeV $\approx (95/R)$ MeV. It is of notice that the elastic vibrational frequency of a spherical solid made out of particles of mass m can be written as $\omega_{el}^2 \sim \mu/(m\rho R^2) \sim v_t^2/R^2$, where R is the radius, ρ the density and v_t the transverse sound velocity proportional to the Lamé shear modulus of elasticity μ . In other words, giant resonance in general, and the GDR in particular, are embodiments of the elastic response of the nucleus to an impulsive external fields, like that provided by a photon. The nuclear rigidity to sudden solicitations is provided by the shell structure, quantitatively measured by the energy separation between major shells.

1.6 Giant pairing vibrations

Due to spatial quantization, in particular to the existence of major shells of pair degeneracy $\Omega (\equiv (2j+1)/2)$, and separated by an energy $\hbar\omega_0 \approx 41/a^{1/3}$ MeV, the Cooper pair model can be extended to encompass pair addition and pair subtraction modes across major shells¹⁶ Assuming both ϵ_k and ϵ_i appearing in Fig. 1.3.1 are both at an energy $\hbar\omega_0$ away from the Fermi energy, one obtains the dispersion relation

$$-\frac{1}{G} = \frac{\Omega}{W - 2\hbar\omega_0} - \frac{\Omega}{W + 2\hbar\omega_0}, \quad (1.6.1)$$

leading to

$$(2\hbar\omega_0)^2 - W^2 = 4\hbar\omega_0 G, \quad (1.6.2)$$

and implying a high lying pair addition mode of energy

$$W = 2\hbar\omega_0 \left(1 - \frac{G\Omega}{\hbar\omega_0}\right)^{1/2}. \quad (1.6.3)$$

The forwards (backwards) going RPA amplitudes are, in the present case

$$X = \frac{\Lambda_0^2 \Omega^{1/2}}{2\hbar\omega_0 - W} \quad \text{and} \quad Y = \frac{\Lambda_0^2 \Omega^{1/2}}{2\hbar\omega_0 + W} \quad (1.6.4)$$

normalized according to the relation

$$1 = X^2 - Y^2 = \Lambda_0^2 \Omega \frac{8\hbar\omega_0 W}{((2\hbar\omega_0)^2 - W^2)^2}, \quad (1.6.5)$$

¹⁶Broglia and Bes (1977).

where Λ_0 stands for the particle-pair vibration coupling vertex. Making use of (1.6.2) one obtains

$$\left(\frac{\Lambda_0}{G}\right)^2 = \Omega \left(1 - \frac{G\Omega}{\hbar\omega_0}\right)^{-1/2} \quad (1.6.6)$$

quantity corresponding, within the framework of the simplified model used, to the two-nucleon transfer cross section. Summing up, the monopole giant pairing vibration has an energy close to $2\hbar\omega_0$, and is expected to be populated in two-particle transfer processes with a cross section of the order of that associated with the low-lying pair addition mode, being this one of the order of Ω . Simple estimates of (1.6.3) and (1.6.6) can be obtained making use of $\Omega \approx \frac{2}{3}A^{2/3}$ and $G \approx 17/A$ MeV lead to

$$W = 0.85 \times 2\hbar\omega_0, \quad \left(\frac{\Lambda_0}{G}\right)^2 \approx 1.2\Omega. \quad (1.6.7)$$

Experimental evidence of GPV in light nuclei have been reported¹⁷

1.7 Sum rules

There are important operator identities which restrict the possible matrix elements in a physical system. Let us calculate the double commutator of the Hamiltonian describing the system and a single-particle operator F . That is

$$[\hat{F}, [H, \hat{F}]] = (2\hat{F}H\hat{F} - \hat{F}^2H - H\hat{F}^2) \quad (1.7.1)$$

Let us assume that $\hat{F} = \sum_k F(\mathbf{r}_k)$ and $H = T + v(\mathbf{r}, \mathbf{r}')$, where $v(\mathbf{r}, \mathbf{r}') = -\kappa_1 \hat{F}(\mathbf{r})\hat{F}(\mathbf{r}')$. Thus

$$[\hat{F}, [H, \hat{F}]] = \sum_k \frac{\hbar^2}{m} (\nabla_k F(\mathbf{r}_k))^2 \quad (1.7.2)$$

Let us take the average value on the correlated ground state

$$S(F) = \sum_{\alpha'} |\langle \alpha' | F | \tilde{0} \rangle|^2 (E_{\alpha'} - E_0) = \frac{\hbar^2}{2m} \int d\mathbf{r} |\nabla F|^2 \rho(\mathbf{r}), \quad (1.7.3)$$

where we have used $H|\alpha\rangle = E_\alpha$ and $H|\tilde{0}\rangle = E_0|\tilde{0}\rangle$, and the sum $\sum_{\alpha'}$ is over the complete set of eigenstates of the system. The above result describes the reaction of a system at equilibrium to which one applies an impulsive field, which gives the particles a momentum ∇F . On the average, the particles started at rest so their average energy after the sudden impulse is $\hbar^2 |\nabla F|^2 / 2m$, a result which is model independent not depending on the interaction among the nucleons, the energy being

¹⁷Cappuzzello et al. (2015); see also Bortignon and Broglia (2016).

absorbed from the (instantaneous) external field before the system is disturbed from equilibrium. The result (1.7.3) is known as the energy weighted sum rule (EWSR).

An important application of (1.7.3) implies a situation where F has a constant gradient. Inserting $\mathbf{F} = z\mathbf{z}$ in (1.7.3), the integral simplifies because $\nabla F = 1$, and the integral leads just to the number of particles,

$$\sum_{\alpha} |\langle \alpha | F | \tilde{0} \rangle|^2 (E_{\alpha} - E_0) = \frac{\hbar^2 N}{2m} \quad (1.7.4)$$

The electric field of a photon is of this form in the dipole approximation, which is valid when the size of the system is small compared to the wavelength of the photon, the single-particle field being

$$F(\mathbf{r}_k) = e \left[\frac{N - Z}{A} - t_z(k) \right] r_k Y_{1\mu}(\hat{r}_k), \quad (1.7.5)$$

with $t_z = -1/2$ for protons and $+1/2$ for neutrons. For the dipole operator referred to the nuclear center of mass one obtains

$$\sum_{\alpha'} |\langle \alpha' | F | \tilde{0} \rangle|^2 (E_{\alpha'} - E_0) = \frac{9}{4\pi} \frac{\hbar^2 e^2}{2m} \frac{NZ}{A}. \quad (1.7.6)$$

The above relation is known as the Thomas-Reiche-Kuhn (TRK) sum rule, and is equal to the maximum energy a system can absorb from the dipole field. The RPA solution respect the EWSR, while the Tamm-Dancoff approximation (TDA), resulting by setting $Y_{ki}^{\alpha} = 0$ and normalizing the X -components ($\sum_{ki} X_{ki}^{\alpha 2} = 1$) fulfill the non-energy weighted sum rule. A fact which testifies to the important role ZPF play in nuclei.

1.8 Ground state correlations

The zero point fluctuations associated with collective vibrations of protons and of neutrons affect the nuclear mean field static properties. In particular concerning the nuclear density distribution¹⁸ ρ and radius R . According to the indeterminacy relations,

$$\Delta \alpha_{\lambda\mu}^{(n)} \Delta \pi_{\lambda\mu}^{(n)} \geq \frac{\hbar}{2}. \quad (1.8.1)$$

Making use of the virial theorem ($\Delta \pi_{\lambda\mu}^2 / D_{\lambda} = C_{\lambda} \alpha_{\lambda\mu}^2$) one can write

$$\Delta \alpha_{\lambda\mu}^{(n)} \geq \frac{\hbar \omega_{\lambda}}{2C_{\lambda}}. \quad (1.8.2)$$

¹⁸Gogny (1978); Esbensen and Bertsch (1983); Reinhard and Drechsel (1979); Khodel et al. (1982); Barranco and Broglia (1987) see also Brown and Jacob (1963); Anderson and Thouless (1962) (it is likely a coincidence in connection with this inaugural issue of Phys. Lett. that short of hundred pages after, one finds the paper of B. D. Josephson, Possible new effects in superconducting tunneling, Phys. Lett. **1**, 251 (1962)).

Let us compare this relation with the expectation value of $\Delta\alpha_{\lambda\mu}^2$ in the ground state of the collective Hamiltonian (1.1.9) described by the wavefunction $\Psi_0(\alpha_{\lambda\mu}^{(n)}) = \left(\frac{D_\lambda^{(n)}\omega_\lambda^{(n)}}{\hbar\pi}\right)^{1/4} \exp\left(-\frac{D_\lambda^{(n)}\omega_\lambda^{(n)}}{2\pi}\alpha_{\lambda\mu}^2\right)$. The result coincides with the lowest limit of (1.8.1) in keeping with the fact that $|\Psi_0|^2$ is mathematically a Poisson distribution¹⁹ The fact that $\Delta\alpha_{\lambda\mu}^2(n) = \hbar\omega_\lambda(n)/2C_\lambda(n)$ implies that the mean square radius will be modified from its mean field value R_0 (Eq. (1.8.1)) and thus also the nuclear density distribution. The value of $\hbar\omega_\lambda(n)/2C_\lambda(n)$ can be determined by calculating the collective mode $|n_\lambda(n)=1\rangle = \Gamma_{\lambda\mu}^\dagger(n)|\tilde{0}\rangle$ in RPA. As seen from the caption to Fig. 1.2.3 the zero point fluctuation of the mode enter the definition of the X, Y -amplitudes of the mode. Let us start by calculating the effect of the zero point fluctuations on the nuclear density distribution. The corresponding operator can be written as

$$\hat{\rho}(\mathbf{r}) = a^\dagger(\mathbf{r})a(\mathbf{r}), \quad (1.8.3)$$

where $a^\dagger(\mathbf{r})$ is the creation operator of a nucleon at point \mathbf{r} . It can be expressed in terms of the phase space creation operators $a_v^\dagger(v \equiv n, l, j, m)$ as

$$a^\dagger(\mathbf{r}) = \sum_v \varphi_v^*(\mathbf{r})a_v^\dagger, \quad (1.8.4)$$

where $\varphi_v(\mathbf{r})$ are the single-particle wavefunctions. Thus

$$\hat{\rho}(\mathbf{r}) = \sum_{v\nu} \varphi_v^*(\mathbf{r})\varphi_{v'}(\mathbf{r})a_v^\dagger a_{v'}. \quad (1.8.5)$$

The matrix element in the HF ground state is (Fig. 1.2.2)

$$\rho_0(\mathbf{r}) =_F \langle 0|\hat{\rho}(\mathbf{r})|0\rangle_F = \sum_{i,(\epsilon_i \leq \epsilon_F)} |\varphi_i(\mathbf{r})|^2. \quad (1.8.6)$$

To lowest order of perturbation theory in the particle-vibration coupling vertex, the NFT diagrams associated with the change of ρ_0 due to ZPF are shown in Fig. 1.8.1.

¹⁹The same result is found for Ψ_n describing a state with n -quanta, and the basis that solutions with $n \gg 1$ behaves as “quasiclassical” or “coherent” states of the harmonic oscillator (Glauber (2007)) in keeping with the fact that the contribution of the zero point energy is negligible in such case ($(n + 1/2)\hbar\omega \approx n\hbar\omega$) and that the many quanta wavepacket always attain the lower limit of (1.8.1) (Basdevant and Dalibard (2005) pp. 153,465) (discussions with Pier Francesco Bortignon in March 2018 concerning coherent states are gratefully acknowledged). Schrödinger was the first to find this result which he used in a paper (Schrödinger, E. (1926)) to suggest that waves (material waves) described by his wave function are the only reality, particles being only derivative things. In support of his view he considered a superposition of linear harmonic oscillator wavefunctions and showed that the wave group holds permanently together in the course of time. And he adds that the same will be true for the electron as it moves in high orbits of the hydrogen atom, hoping that wave mechanics would turn out to be a branch of classical physics (Pais (1986)). It was Born who first provided the correct interpretation of Schrödinger’s wavefunction (modulus square) in his paper “Quantum mechanical collision phenomena” (Born (1926)). In it it is stated that the result of solving with wave mechanics the process of elastic scattering of a beam of particles by a static potential is not what the state after the collision is, but how probable is a given effect of the collision.

Graphs (a) and (b) and (c) and (d) describe the changes in the density operator and in the single-particle potential respectively. This can be seen from the insets (I) and (II). The dashed horizontal line starting with a cross and ending at a hatched circle represents the renormalized density operator. This phenomenon is similar to that encountered in connection with vertex renormalization in Fig. 1.2.5, that is the renormalization of the particle-vibration coupling (insets (I) and (I')). Concerning potential renormalization, the bold face arrowed line shown in inset (II) of Fig. 1.8.1 represents the motion of a renormalized nucleon due to the self-energy process induced by the coupling to vibrational modes. A phenomenon which can be described at profit through an effective mass, the so called ω -mass m_ω , in which case particle motion is described by the Hamiltonian²⁰ $(\hbar^2/2m_\omega)\nabla^2 + (\frac{m}{m_\omega})U(r)$. The ω -mass can be written as $m_\omega = (1 + \lambda)m$, where λ is the so called mass enhancement factor $\lambda = N(0)\Lambda$, where $N(0)$ is the density of levels at the Fermi energy, and Λ the PVC vertex strength, typical values being $\lambda = 0.4$.

The fact that in calculating $\delta\rho$, that is, the correction to the nuclear density distribution (renormalization of the density operator), one finds to the same order of perturbation a correction to the potential, is in keeping with the self consistency existing between the two quantities (Eq. (1.2.6)). Now, what changes is not only the single-particle energy, but also the single-particle content as well as the radial dependence of the wavefunctions of the states measured by $Z_\omega = m/m_\omega$. It is of notice that the effective mass approximation, although being quite useful, cannot take care of the energy dependence of the renormalization process which leads, in the case of single-particle motion to renormalized energies, spectroscopic amplitudes and wavefunctions. The analytic expressions associated with diagrams (a) and (c) of Fig. 1.8.1 are

$$\delta\rho(r)_{(a)} = \frac{(2\lambda + 1)}{4\pi} \sum_{\nu_1\nu_2n} [Y_n(\nu_1\nu_2; \lambda)]^2 R_{\nu_1}(r)R_{\nu_2}(r), \quad (1.8.7)$$

and

$$\begin{aligned} \delta\rho(r)_{(b)} &= (2\lambda + 1)\Lambda_n(\lambda) \sum_{\nu_1\nu_2\nu_3} \frac{M(\nu_1, \nu_3; \lambda)}{\epsilon_{\nu_1} - \epsilon_{\nu_2}} (2j_1 + 1)^{-1/2} \\ &\times Y_n(\nu_3\nu_2; \lambda) \times R_{\nu_1}(r)R_{\nu_2}(r), \end{aligned} \quad (1.8.8)$$

where M is the matrix element of $\frac{R_0}{\kappa} \frac{\partial U}{\partial r} Y_{\lambda\mu}(\hat{r})$ and $n = 1, 2 \dots$ the first, second, etc vibrational modes as a function of increasing energy, and Λ_n is the strength of the particle-vibration coupling associated with the n -mode of multipolarity λ . While $\delta\rho_{(a)}$ can be written in terms of the RPA Y -amplitudes which are directly associated with the zero point fluctuations of harmonic motion (Fig. 1.2.3 (c)), $\delta\rho_{(c)}$ contains a scattering vertex not found in RPA – that is going beyond the harmonic approximation – and essential to describe renormalization processes of the different degrees of freedom, namely single-particle (energy, single-particle

²⁰Brink, D. and Broglia (2005).

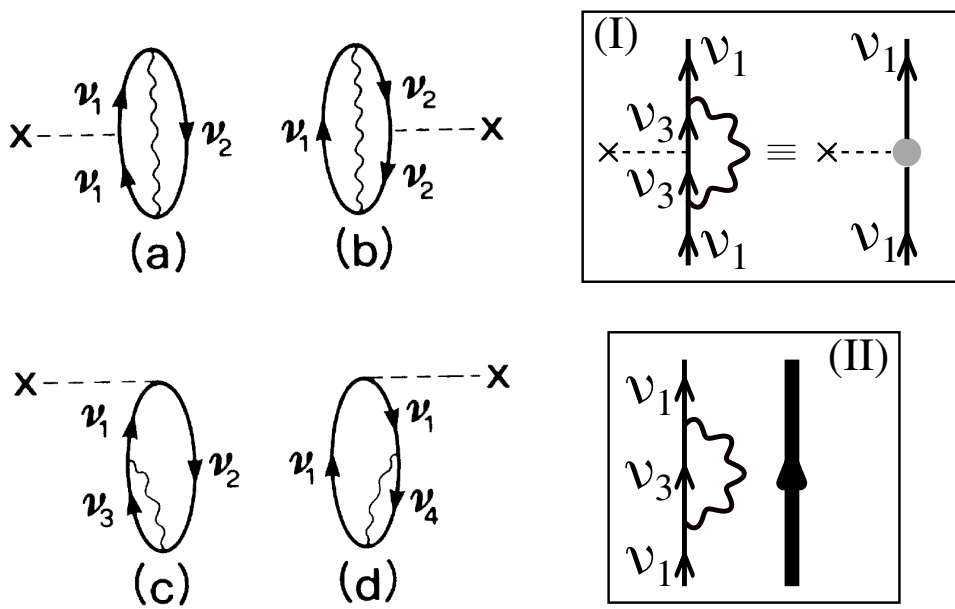


Figure 1.8.1: Lowest-order corrections in the particle-vibration coupling vertex of the nuclear density due to the presence of zero-point fluctuations associated with density vibrations. An arrowed line pointing upwards denotes a particle, while one pointing downward a hole. A wavy line represents a surface phonon. The density operator is described through a dotted horizontal line starting with a cross. Graphs (a) and (b) are typical examples of density contributions to $\delta\rho$ (see inset (I)); the dashed horizontal line starting with a cross and ending at a hatched circle in the diagram to the right, represents the renormalized density operator, resulting from the processes displayed to the left; (c) and (d) are of potential contributions (see inset (II)); the bold face arrowed line represents the renormalized single-particle state due to the coupling to the vibrations leading to the self energy process shown to the left. (After Barranco and Broglia (1987)).

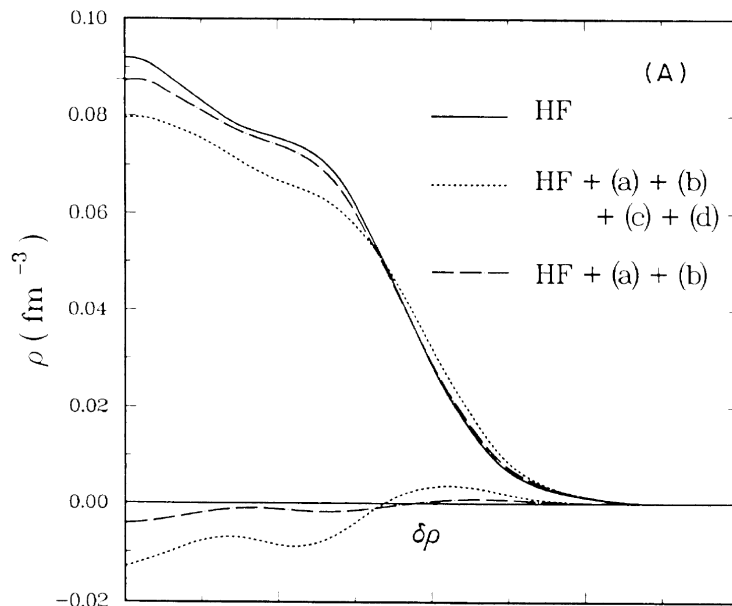


Figure 1.8.2: Modification in the charge density of ^{40}Ca induced by the zero-point fluctuations associated with vibrations of the surface modes. The results labeled HF, HF+(a)+(b), and HF+(a)+(b)+(c)+(d) are the Hartree-Fock density, and that resulting from adding to it the corrections $\delta\rho$ associated with the processes (a)+(b) and (a)+(b)+(c)+(d) displayed in Fig. 1.8.1, respectively. In the lower part of the figure the quantities $\delta\rho$ are displayed. (After Barranco and Broglia (1987)).

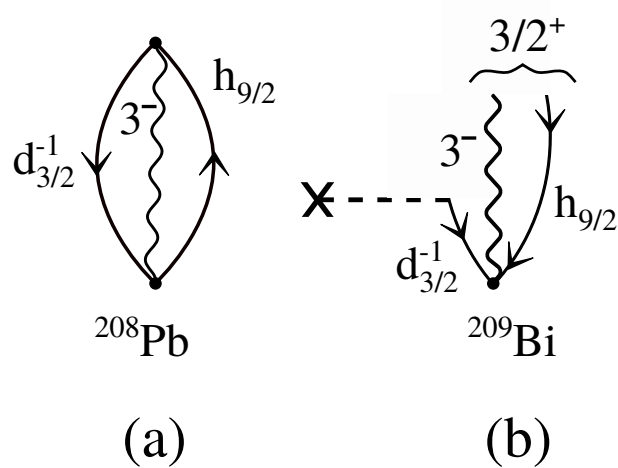


Figure 1.8.3: (a) Example of zero point fluctuation of the ground state of the double-magic nucleus $^{208}_{82}\text{Pb}_{126}$ associated with the low-lying octupole vibration of this system, observed at an energy of 2.615 MeV and displaying a collective electromagnetic decay to the ground state. The proton particle-hole component $(h_{9/2}, d_{3/2}^{-1})_{3^-}$ displayed carries a large amplitude in the octupole vibration wavefunction. (b) Diagram representing the transfer of one proton to ^{208}Pb , which fills the $d_{3/2}^{-1}$ hole state leading to a $3/2^+$ in $^{209}_{83}\text{Bi}_{126}$, member of the septuplet of states $|(3^- \otimes h_{9/2} J^\pi)\rangle$ with $J^\pi = 3/2^+, 5/2^+, \dots, 15/2^+$. The horizontal dashed line starting with a cross stands for the stripping process $(^3\text{He}, d)$.

content and radial dependence of the wavefunction) and collective motion, as well as interactions. In particular the pairing interaction.

In Fig. 1.8.2 we show the results of calculations of $\delta\rho$ carried out for the closed shell nucleus ^{40}Ca . The vibrations were calculated by diagonalizing separable interactions of multipolarity λ in the RPA. All the roots of multipolarity and parity $\lambda^\pi = 2^+, 3^-, 4^+$ and 5^- which exhaust the EWSR were included in the calculations. Both isoscalar and isovector degrees of freedom were included, and low-lying and giant resonances.

From the point of view of the single-particle motion the vibrations associated with low-lying modes display very low frequency ($\hbar\omega_\lambda/\epsilon_F \approx 0.1$) and lead to an ensemble of deformed shapes. Nucleons can thus reach to distances from the nuclear center which are considerably larger than the radius R of the static spherical potential. Because the frequency of the giant resonances are of similar magnitude to those corresponding to the single-particle motion, the associated surface deformations average out.

Said it differently, the low-lying vibrational modes account for most of the contributions to the changes in the density distribution²¹. Making use of the corresponding $(\delta\rho)_{low-lying}$, the mean square radius of ^{40}Ca was calculated²², leading to $\langle r^2 \rangle = (3/5)R_0^2 = 10.11 \text{ fm}^2$ ($R_0 = 1.2A^{1/3} \text{ fm} = 4.1 \text{ fm}$), in overall agreement with the experimental findings. Similar calculations to the ones discussed above, but in this case taking into account only the contributions of the low-lying octupole vibration²³ indicate that nucleons are to be found a reasonable part of the time in higher shells than those assigned to them by the shell model. The average number of “excited” particles being ≈ 2.4 . If these are present, pickup reactions such as (p, d) and (d, t) will show them. From the nature of the correlations, the pickup of such a particle will leave a hole and a vibration. That is, the final nucleus will be in one of the states which can be related by coupling the hole and the vibration. Conversely, because of the presence of hole states in the closed shell nucleus, one can transfer a nucleon to states below the Fermi energy in, for example, (d, p) or $(^3\text{He}, d)$ one-neutron or one-proton stripping reactions respectively, leaving the final nucleus with one-nucleon above closed shell coupled to the vibrations.

Systematic studies of such multiplets have been carried out throughout the mass table. In particular around the closed shell nucleus $^{208}_{82}\text{Pb}_{126}$ (Fig. 1.8.3). Within this context it is not only quite natural but also necessary, to deal with structure and reactions on equal footing. This is one of the main goals of the present monograph, as will become clear already from the next chapter.

²¹Another example of the recurrent central role played by low-frequency modes in determining the properties and behavior of systems at all levels of organization, from the atomic nucleus to the Casimir effect in QED, to phonons in superconductors as well as to the folding of proteins and brain activity ($\nu < 0.1 \text{ Hz}$) (Mitra et al. (2018)).

²²Barranco and Broglia (1987).

²³Brown and Jacob (1963).

Bibliography

- P. Anderson and D. Thouless. Diffuseness of the nuclear surface. *Physics Letters*, 1(5):155 – 157, 1962.
- J. Bardeen, L. N. Cooper, and J. R. Schrieffer. Microscopic theory of superconductivity. *Physical Review*, 106:162, 1957a.
- J. Bardeen, L. N. Cooper, and J. R. Schrieffer. Theory of superconductivity. *Physical Review*, 108:1175, 1957b.
- F. Barranco and R. A. Broglia. Effect of surface fluctuations on the nuclear density. *Phys. Rev. Lett.*, 59:2724, 1987.
- F. Barranco, R. A. Broglia, G. Colò, G. Gori, E. Vigezzi, and P. F. Bortignon. Many-body effects in nuclear structure. *European Physical Journal A*, 21:57, 2004.
- J. L. Basdevant and J. Dalibard. *Quantum Mechanics*. Springer, Berlin, 2005.
- G. F. Bertsch, P. F. Bortignon, and R. A. Broglia. Damping of nuclear excitations. *Rev. Mod. Phys.*, 55:287, 1983.
- A. Bohr and B. R. Mottelson. *Nuclear Structure, Vol.I*. Benjamin, New York, 1969.
- A. Bohr, B. R. Mottelson, and D. Pines. Possible analogy between the excitation spectra of nuclei and those of the superconducting metallic state. *Physical Review*, 110:936, 1958.
- N. Bohr and J. A. Wheeler. The mechanism of nuclear fission. *Phys. Rev.*, 56:426, 1939.
- Bohr, A. and B. R. Mottelson. *Nuclear Structure, Vol.II*. Benjamin, New York, 1975.
- M. Born. Zur Quantenmechanik der Stoßvorgänge. *Zeitschr.f. Phys.*, 37:863, 1926.
- P. Bortignon and R. Broglia. Elastic response of the atomic nucleus in gauge space: Giant pairing vibrations. *The European Physical Journal A*, 52(9):280, 2016.

- P. F. Bortignon and R. A. Broglia. Role of the nuclear surface in an unified description of the damping of single-particle states and giant resonances. *Nucl. Phys. A*, 371:405, 1981.
- Bortignon, P. F., A. Bracco, and R. A. Broglia. *Giant Resonances*. Harwood Academic Publishers, Amsterdam, 1998.
- Brink, D. and R. A. Broglia. *Nuclear Superfluidity*. Cambridge University Press, Cambridge, 2005.
- R. A. Broglia and D. R. Bes. High-lying pairing resonances. *Physics Letters B*, 69: 129, 1977.
- R. A. Broglia and A. Winther. *Heavy Ion Reactions*. Westview Press, Boulder, CO., 2004.
- G. Brown and G. Jacob. Zero-point vibrations and the nuclear surface. *Nuclear Physics*, 42:177 – 182, 1963.
- F. Cappuzzello, D. Carbone, M. Cavallaro, M. Bondí, C. Agodi, F. Azaiez, A. Bonaccorso, A. Cunsolo, L. Fortunato, A. Foti, S. Franchoo, E. Khan, R. Linares, J. Lubian, J. A. Scarpaci, and A. Vitturi. Signatures of the Giant Pairing Vibration in the ^{14}C and ^{15}C atomic nuclei. *Nature Communications*, 6: 6743, 2015.
- P. A. M. Dirac. *The principles of quantum mechanics*. Oxford University Press, London, 1930.
- W. Elsasser. Sur le principe de Pauli dans les noyaux. *J. Phys. Radium*, 4:549, 1933.
- H. Esbensen and G. F. Bertsch. Nuclear surface fluctuations: Charge density. *Phys. Rev. C*, 28:355, 1983.
- Flynn, E. R., G. J. Igo, and R. A. Broglia. Three-phonon monopole and quadrupole pairing vibrational states in ^{206}Pb . *Phys. Lett. B*, 41:397, 1972.
- R. J. Glauber. *Quantum theory of optical coherence*. Wiley, Weinheim, 2007.
- D. Gogny. Lecture notes in physics, vol. 108. In H. Arenhövd and D. Drechsel, editors, *Nuclear Physics with Electromagnetic Interactions*, p.88, page 55, Heidelberg, 1978. Springer Verlag.
- O. Haxel, J. H. D. Jensen, and H. E. Suess. On the “Magic Numbers” in nuclear structure. *Phys. Rev.*, 75:1766, 1949.
- V. A. Khodel, A. P. Platonov, and E. E. Saperstein. On the 40ca-48ca isotope shift. *Journal of Physics G: Nuclear Physics*, 8(7):967–973, jul 1982.

- E. Litvinova and H. Wibowo. Finite-temperature relativistic nuclear field theory: An application to the dipole response. *Phys. Rev. Lett.*, 121: 082501, Aug 2018. doi: 10.1103/PhysRevLett.121.082501. URL <https://link.aps.org/doi/10.1103/PhysRevLett.121.082501>.
- M. Mayer and J. Jensen. *Elementary Theory of Nuclear Structure*. Wiley, New York, NY, 1955.
- M. G. Mayer. On closed shells in nuclei. *Phys. Rev.*, 74:235, 1948.
- M. G. Mayer. On closed shells in nuclei. ii. *Phys. Rev.*, 75:1969, 1949.
- M. G. Mayer. The shell model. *Nobel Lecture*, 1963.
- M. G. Mayer and E. Teller. On the origin of elements. *Phys. Rev.*, 76:1226, 1949.
- L. Meitner and O. R. Frisch. Products of the fission of the uranium nucleus. *Nature*, 143:239, 1939.
- A. Mitra, A. Kraft, P. Wright, B. Acland, A. Z. Snyder, Z. Rosenthal, L. Czerniewski, A. Bauer, L. Snyder, J. Culver, et al. Spontaneous infra-slow brain activity has unique spatiotemporal dynamics and laminar structure. *Neuron*, 98: 297, 2018.
- Y. Nambu. Quasi-particles and gauge invariance in the theory of superconductivity. *Physical Review*, 117:648, 1960.
- O. Nathan and S. G. Nilsson. Collective nuclear motion and the unified model. In K. Siegbahn, editor, *Alpha- Beta- and Gamma-Ray Spectroscopy, Vol 1*, page 601, Amsterdam, 1965. North Holland Publishing Company.
- S. G. Nilsson. Binding states of individual nucleons in strongly deformed nuclei. *Mat. Fys. Medd. Dan. Vid. Selsk.*, 29, 1955.
- P. J. Nolan and P. J. Twin. Superdeformed shapes at high angular momentum. *Annual Review of Nuclear and Particle Science*, 38:533, 1988.
- A. Pais. *Inward bound*. Oxford University Press, Oxford, 1986.
- Potel, G., A. Idini, F. Barranco, E. Vigezzi, and R. A. Broglia. Quantitative study of coherent pairing modes with two-neutron transfer: Sn isotopes. *Phys. Rev. C*, 87:054321, 2013.
- P. G. Reinhard and D. Drechsel. Ground state correlations and the nuclear charge distribution. *Zeitschrift für Physik A Atoms and Nuclei*, 290(1):85–91, Mar 1979.
- D. J. Rowe. *Nuclear Collective Motion. Models and Theory*. Methuen & Co., London, 1970.

- Schiffer, J. P., C. R. Hoffman, B. P. Kay, J. A. Clark, C. M. Deibel, S. J. Freeman, A. M. Howard, A. J. Mitchell, P. D. Parker, D. K. Sharp, and J. S. Thomas. Test of sum rules in nucleon transfer reactions. *Phys. Rev. Lett.*, 108:022501, 2012.
- Schrödinger, E. *Naturw.*, 14:644, 1926.
- J. C. Ward. An identity in quantum electrodynamics. *Phys. Rev.*, 78:182–182, Apr 1950. doi: 10.1103/PhysRev.78.182. URL <https://link.aps.org/doi/10.1103/PhysRev.78.182>.
- C. F. Weizsäcker. Zur theorie der kernmassen. *Z. Phys.*, 96:431, 1935.
- H. Wibowo and E. Litvinova. Nuclear dipole response in the finite-temperature relativistic time-blocking approximation. *Phys. Rev. C*, 100:024307, Aug 2019. doi: 10.1103/PhysRevC.100.024307. URL <https://link.aps.org/doi/10.1103/PhysRevC.100.024307>.